STI OPTRONICS

LASER WAKEFIELD ACCELERATION DRIVEN BY A CO_2 LASER (STELLA-LW)

Final Report

Submitted to
U. S. Department of Energy

Submitted by
STI Optronics, Inc.

June 27, 2008

1828.6

LASER WAKEFIELD ACCELERATION DRIVEN BY A CO_2 LASER (STELLA-LW)

Final Report for
Contract No. DE-FG02-04ER41294

Submitted to:
U. S. Department of Energy

by

STI Optronics, Inc.
2755 Northup Way
Bellevue, Washington 98004-1495

Dr. Wayne D. Kimura
Principal Investigator

Lorrie W. Sanborn
Contract Administrator

Telephone: (425) 827-0460
Facsimile: (425) 828-3517
e-mail: wkimura@stioptronics.com

June 27, 2008

TABLE OF CONTENTS

SECTION 1
EXECUTIVE SUMMARY

The original goals of the Staged Electron Laser Acceleration – Laser Wakefield (STELLA-LW) program were to investigate two new methods for laser wakefield acceleration (LWFA). The first method is called pseudo-resonant LWFA (PR-LWFA) in which a laser pulse experiences nonlinear pulse steepening while traveling through the plasma. This steepening allows the laser pulse to generate wakefields even though the laser pulse length is too long for resonant LWFA to occur. For the conditions of this program, PR-LWFA requires a minimum laser peak power of 3 TW and a relatively low plasma density of order 10^{16} cm^{-3}.

The second method is a hybrid one that combines LWFA with plasma wakefield acceleration (PWFA) and is called seeded self-modulated LWFA (seeded SM-LWFA). In this method, an ultrashort (~100 fs) electron beam (*e*-beam) bunch acts as a seed in a plasma to form a wakefield via PWFA. This wakefield is subsequently amplified by the laser pulse through a self-modulated LWFA process. In order to cause the self-modulation effect, a minimum of 1 TW laser power is needed. Furthermore, for a ~100-fs bunch, a plasma density of order 10^{17} cm^{-3} is required.

STELLA-LW was located on Beamline #1 at the Brookhaven National Laboratory (BNL) Accelerator Test Facility (ATF). The ATF TW CO_2 laser served as the driving laser beam for both methods. For PR-LWFA, the plan was for the ATF linac to provide its standard bunch to probe the wakefield produced by the laser beam. For seeded SM-LWFA, the plan was for the ATF linac to produce two bunches where the first bunch would act as the seed and the second bunch would serve as a witness bunch. These two bunches can be created by sending two laser pulses to the photocathode *e*-gun of the ATF linac. A chicane would also be used during seeded SM-LFWA to compress the first bunch to enable it to generate wakefields via PWFA. The plasma source was a short-length, gas-filled capillary discharge in which the laser beam was tightly focused in the center of the capillary, i.e., no laser guiding was used. This was done in order to obtain the required laser intensity to drive the LWFA process.

During the course of the program, we had to make several major changes to our approach. First, it became clear due to funding limitations that the ATF could not complete within the time period of the STELLA-LW program the upgrade of the CO_2 laser to the 3 TW peak power needed for the PR-LWFA experiment. Therefore, the PR-LWFA experiment had to be abandoned and all efforts focused on performing the seeded SM-LWFA experiment.

Second, when the ATF tested the chicane for creating the compressed bunch, it was discovered that the incoming bunch bifurcated into two compressed bunches with comparable bunch lengths, but separated in time (~1 ps) and energy (~1.8 MeV). It appears this is caused by a complex interaction between the chicane and two dogleg dipoles located between the chicane and the STELLA-LW experiment on Beamline #1. Moreover, it was found there is no simple way to prevent the double bunches from being formed, and the separation distance and energy difference could not be changed.

Separate experiments demonstrated that the double-bunches are capable of generating wakefields, but in a complex manner where the wakefield from the second bunch can interfere constructively or destructively with the wakefield from the first bunch. In an attempt to still deliver a single compressed bunch to the experiment, it was decided to use a slit located at a high

dispersion point along the linac to block one of the bunches. However, this slit would also block any witness bunch.

This brings us to the third major change. The loss of the witness bunch meant we had to find a different method for detecting the effect of the laser beam on the wakefield produced by the seed bunch. Coherent Thomson scattering (CTS), whereby Stokes and anti-Stokes sidebands of the fundamental laser beam are generated by scattering of light off the wakefield, can give a indirect indication of the presence of the wakefield and its strength. Thus, a CTS diagnostic was designed and assembled for the seeded SM-LWFA experiment.

Unfortunately, further tests with blocking one of the double-bunches showed that wakefield generation was unstable and difficult to control due to the nonlinear nature of the double-bunch formation process and the inability to reliably reproduce the same compressed bunch characteristics. Luckily, it was found that the *e*-beam optics along Beamline #2 at the ATF could be tuned so that the leading edge of the 1-ps bunch produced by the linac is sharpen to a rise-time of order 50 fs. This fast-rising leading edge is capable of generating wakefields and does not require using the chicane. Moreover, this pulse steepening process yields a much more stable bunch than from the chicane. Model simulations indicated using this type of bunch for PWFA generation would still enable demonstration of seeded SM-LWFA.

Therefore, as the fourth and final major change in the experiment, the entire STELLA-LW apparatus, including the CTS diagnostic, was moved from Beamline #1 to Beamline #2. Because this move occurred near the end of the program, there was only enough time for a single 2-week run that would have to include completion of the move, realignment of the optics, and performing the integrated experiment.

During the experiment on Beamline #2, the laser beam transmission passing through the capillary discharge was monitored. We found the transmission was severely degraded when the plasma was on. This loss of transmission appeared to be due to defocusing of the laser beam most likely caused by laser-induced ionization creating a lens effect inside the capillary. Defocusing could also cause laser light to strike the capillary wall, thereby producing ablation and localized changes in the plasma density. Any changes in the plasma density would disrupt the plasma resonance condition for the wakefield. It was also discovered after the run that the ATF laser was producing multiple output pulses. The leading pulse could have caused ionization that interfered with transmission of the following pulses. Worse yet, the peak power in each of the pulses was several times smaller than if all the pulse energy was in a single pulse. This meant each pulse had less than 1 TW power.

Wakefield formation with no laser beam present was confirmed by observing energy loss of the fast-raising seed bunch passing through the capillary discharge. When the laser beam was sent into the plasma, no CTS signal was detected probably because of defocusing of the laser light, changes in the plasma density due to laser-induced ionization, and insufficient peak power in the individual pulses. It is for these reasons we were not able to validate the seeded SM-LWFA predictions.

As mentioned, the Beamline #2 run occurred at the end of the STELLA-LW performance period and, hence, no further experimental work was pursued. It should be emphasized that the failure to detect CTS radiation does not imply the seeded SM-LWFA theory is invalid. The aforementioned major changes in the experimental approach ultimately forced us into conditions

that deviated too much away from the modeling work. Hence, the experiment as finally performed was not a true test of the theory.

In principle, one way to address the problem of laser-induced ionization would be to design the capillary to guide the laser beam. Unfortunately, it is unlikely this would have helped us. The on-axis plasma density is dictated by the seed bunch rise-time and had to be relatively low ($\sim 10^{17}$ cm^{-3}). The depth of the parabolic density profile for guiding the laser beam is affected by the on-axis density and becomes shallower at lower densities. The matched laser beam waist for guiding tends to become larger as the depth becomes shallower. In our case, the required matched laser waist for the available laser power would yield too low of a laser intensity inside the capillary to drive the SM-LWFA process. The only way to rectify this situation is to have higher laser peak power, which was not available.

In summary, the STELLA-LW experiment was not able to demonstrate seeded SM-LWFA or PR-LWFA primarily because of limitations of the ATF CO_2 laser, both in its deliverable peak power and its ability to provide a single laser pulse.

One outcome of this experiment is that improved capillary discharges are needed whose parameters allow more flexibility in the capillary design and, in particular, offer designs that are able to guide tightly-focused laser beams at relatively low plasma densities. This need was part of the impetus for a new proposal that has been submitted to the U.S. Department of Energy to develop advanced capillary discharges. These advanced capillary designs utilize two new, innovative approaches that may enable better operation at low plasma densities and relieve the problem of gas-loading of the linac beamline vacuum from gas emitted by the discharge.

The next section, Sec. 2, reviews the entire STELLA-LW program in more detail, including the theory, description and results of the experiment, collaborations with other experiments, and briefly reviews the proposed ideas for improving the capillary discharge as mentioned above. Section 3 lists the publications and presentations associated with the STELLA-LW program and our collaborations with others.

SECTION 2

STELLA-LW EXPERIMENT

2.1 INTRODUCTION

Laser wakefield acceleration (LWFA) has demonstrated very high acceleration gradients in numerous experiments [2-1]. LWFA is typically initiated by sending a few tens of terawatt (TW) laser pulse into a plasma to create longitudinal plasma waves or wakefields [2-2]. These waves travel at near the speed of light and can accelerate electrons trapped within their potential well. When the laser pulse length τ_L is less than of order $\lambda_p/2c$, where λ_p is the plasma wavelength and c is the speed of light, this wakefield generation is referred to as resonant LWFA.

In a variation of the LWFA method, called self-modulated LWFA (SM-LWFA) [2-3], the laser pulse length is much longer than $\lambda_p/2c$, but the laser intensity is still very high. This permits the laser electric field to feed energy into the wakefield via forward Raman scattering (FRS) and/or a self-modulation instability. This enhances the wakefield formation process allowing much higher gradients to be produced compared to resonant LWFA. However, for wakefield amplitudes of interest, SM-LWFA is a highly nonlinear process that typically starts from noise, so that the phase of the resulting wake is essentially uncontrolled.

Wakefield formation in a plasma is also possible by using an ultrashort electron beam (*e*-beam) bunch rather than a laser pulse. This is referred to as plasma wakefield acceleration (PWFA) [2-4]. The formation mechanism in PWFA is analogous to resonant LWFA; hence, the resultant wakefields can have similar characteristics.

Despite the tremendous progress made in laser acceleration research, there has been limited work to address the pragmatic problem of devising ways to make a useful laser-driven accelerator (laser linac). For efficient acceleration, the electrons must be grouped together (i.e., microbunched) within a small fraction of the accelerating wave phase (e.g., $<\pi/2$). This is important in order for a large percentage of the electrons to be captured ("trapped") within a laser field ponderomotive potential well ("bucket") or plasma wave, such as in LWFA or PWFA. During the acceleration process, the trapped electrons need to maintain a narrow energy spread (i.e., monoenergetic) so that in subsequent laser acceleration devices ("stages") the electrons can continue to be efficiently trapped and accelerated. This staging process whereby laser beams or wakefields repeatedly accelerate the electrons is important for achieving high net acceleration.

It was the goal of our earlier experiment, called Staged Electron Laser Acceleration (STELLA), to demonstrate all these features in a single system. To accomplish this we chose as our basic approach the concept of imparting a sinusoidal energy modulation on the *e*-beam, thereby leading to microbunching, and followed by monoenergetic acceleration with high trapping efficiency. Thus, this earlier experiment was fundamentally about validating a specific process for making a practical laser linac; it was not about further developing a particular laser acceleration mechanism.

Figure 2-1 illustrates this microbunching process using a model simulation for the conditions of the STELLA experiment. Since the *e*-beam pulse length is typically much longer than the accelerating wavelength, the electrons initially enter uniformly distributed over all phases of the acceleration wave [Fig. 2-1(a)]. Exposing the electrons to an oscillating electromagnetic field causes sinusoidal energy modulation of the *e*-beam energy [Fig. 2-1(b)]. If

these electrons are allowed to either drift or are sent through a bunch compressor device (i.e., chicane), then the fast electrons catch up with the slow ones [Fig. 2-1(c)] resulting in the creation of microbunches [Fig. 2-1(d)]. These microbunched electrons can be sent through a second laser accelerator device at the proper phase with respect to the accelerating field in the second device to trap and accelerate the electrons while maintaining a narrow energy spread.

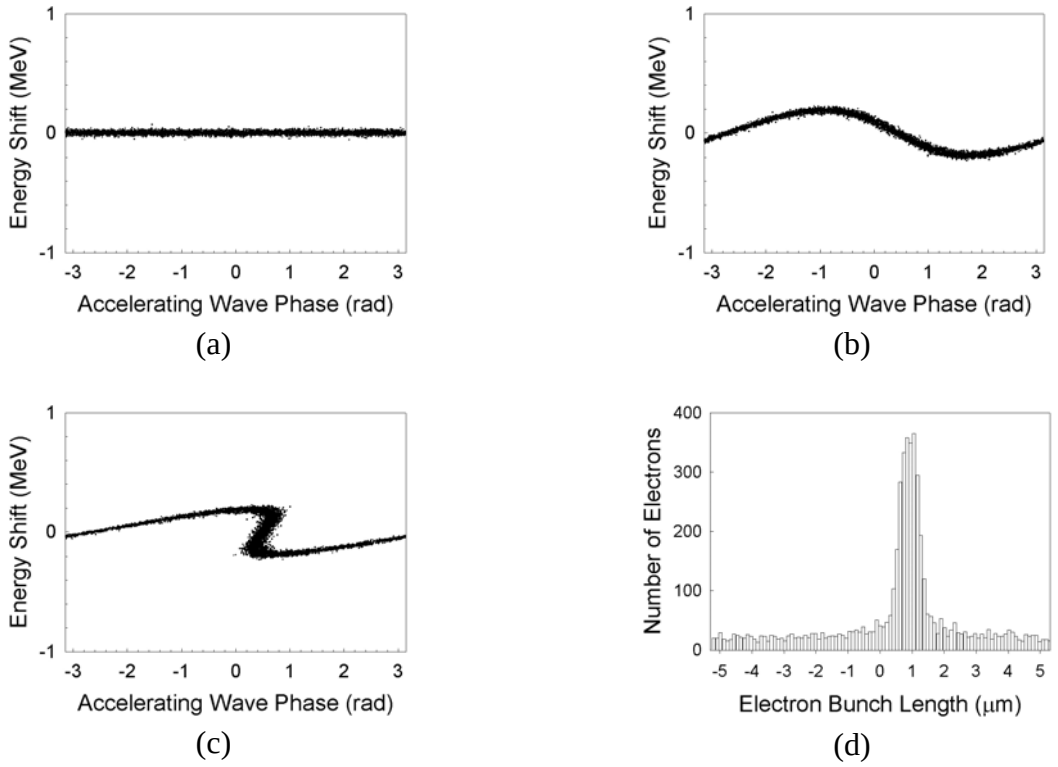

Fig. 2-1. Model simulation for STELLA showing microbunching process. (a) E-beam energy shift from initial energy versus phase distribution relative to accelerating wave. (b) Energy-phase distribution after energy modulation by first laser acceleration stage. (c) Energy-phase distribution after traveling through bunch compressor (chicane) (d) Microbunch longitudinal density distribution of (c).

The basic STELLA concept can be applied to many different laser acceleration schemes. For experimental expediency and simplicity we chose to use inverse free electron lasers [2-5] (IFEL) as our laser acceleration mechanism. An IFEL is a free electron laser operating in reverse. The laser beam co-propagates with the *e*-beam within the gap between a pair of parallel-facing magnet arrays called an undulator. Depending on the sign of the laser field seen by an electron, the electron will be accelerated or decelerated.

The STELLA experiment [2-6], [2-7] used two IFELs operated in series along the electron beamline. The first IFEL served as the buncher to modulate the energy of the incoming *e*-beam. A chicane immediately followed the first IFEL to microbunch the electrons before they entered the second IFEL. In the second IFEL, the electrons were rephrased with the laser field in the second undulator in order to trap and accelerate them. Trapping efficiencies of up to 80% and energy spreads down to 0.36% (1σ) were demonstrated. Building upon the success of the STELLA IFEL experiments, the STELLA-LW experiment goal was to apply the STELLA process to LWFA. (The suffix "LW" stands for "laser wakefield.")

Key to this effort was the goal to generate wakefields whose phase can be reliably controlled. This ruled out the usual SM-LWFA process, which starts from noise. Resonant LWFA should provide more controllable wakefields, but the acceleration gradient from resonant LWFA tends to be much lower than for SM-LWFA. Therefore, during the STELLA-LW program we devised two new LWFA methods – seeded SM-LWFA [2-8] and pseudo-resonant LWFA [2-9], [2-10].

STELLA-LW was located at the Brookhaven National Laboratory (BNL) Accelerator Test Facility (ATF). It was originally positioned on Beamline #1; the same one used for the IFEL experiments. The laser for driving the LWFA process was the ATF TW CO_2 laser, which is capable of 1 TW peak power (i.e., 5 J in 5 ps). A capillary discharge acted as the plasma source. The ATF features a photocathode *e*-gun feeding into an S-band (2856 MHz) linear accelerator. During our experiments the *e*-beam energy was typically 60 MeV.

2.2 NEW LWFA ACCELERATION METHODS

2.2.1 Seeded SM-LWFA

The theory and modeling for seeded SM-LWFA is covered in detail in [2-8] (see Appendix A). Seeded SM-LWFA was originally called stimulated LWFA [2-11] and is a close cousin of Raman seeding [2-12], [2-13]. The latter uses a second low-intensity frequency-shifted laser pulse, which provides a seed for the main laser pulse self-modulation and does not rely on noise to generate the wakefields. In seeded SM-LWFA, an ultrashort *e*-beam bunch precedes the laser pulse to generate a moderate strength wakefield that the laser pulse subsequently amplifies via a self-modulation process. It thus can be viewed as a hybrid technique that combines both PWFA and LWFA. A key aspect of this technique is that the wakefield generated by the seed *e*-beam bunch does not start from noise as is typically the case in SM-LWFA. Instead, the modeling simulations indicate the wakefield phase is closely tied to the arrival time of the seed bunch. The laser pulse simply amplifies this wakefield without significantly changing its phase. Thus, this method may enable more controllable wakefield generation, thereby greatly facilitating the staging of these devices. A witness bunch would nominally follow the laser pulse to probe the amplified wakefield.

Details of the seeded SM-LWFA modeling and its predictions for the ATF are given in Appendix A. Highlights are reviewed here.

The LWFA code, developed by Dr. Nikolai Andreev and his colleagues, was modified by adding seed and witness *e*-beam bunches. Figure 2-2 shows the relationship between these two bunches, the laser pulse (with and without the seed bunch), and the resultant wakefield generation and amplification. We observe the wakefield generation begins with the arrival of the seed bunch. Self-modulation of the laser pulse starts to occur once the wakefield begin to emerge. Consequently, the wakefield potential also increases in magnitude. In this particular example, the witness bunch probes the wakefields 12 ps after the seed.

Figure 2-3 shows the predicted energy spectrum of the witness bunch for an acceleration length of 2 mm and at different time delays between the seed and witness bunches. The spectrum shows fairly symmetric double-peaks caused by energy modulation of the witness electrons distributed over all phases of the wakefield. It is very similar to the modulation observed during the STELLA program when using IFELs [2-14]. In fact, if these energy-modulated electrons are allowed to drift or sent through a chicane, they would form microbunches just as during the earlier STELLA experiment. The key difference is the

microbunches would be spaced apart by the plasma wavelength (~300 μm) instead of the laser wavelength (10.6 μm) and they would have a bunch length of roughly ~30 μm rather than ~1 μm. These microbunches would be well suited for injecting into subsequent LWFA devices for trapping and further acceleration, again analogous to what was demonstrated during the STELLA program with IFELs.

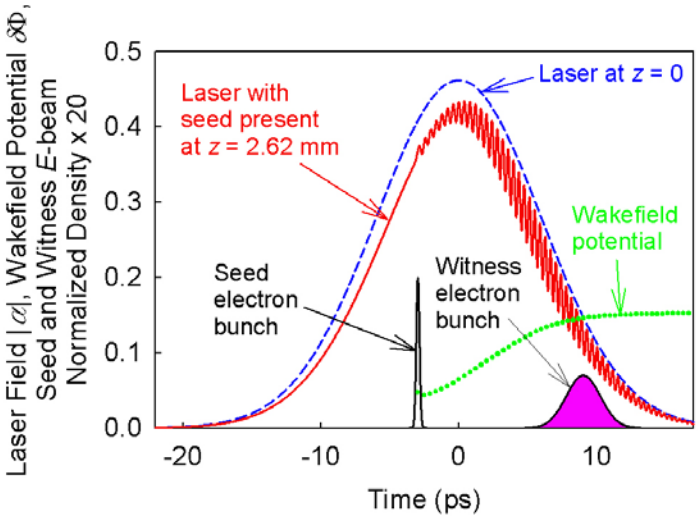

Fig. 2-2. Model prediction for laser field parameter |a(r = 0)| and wakefield potential δΦ (r = 0) as a function of time for z = 2.62 mm and t_d = 2.97 ps. Also plotted are the seed and witness e-beam bunch positions for τ_d = 12 ps, and |a(r = 0, z = 0)|. See Appendix A for more explanations.

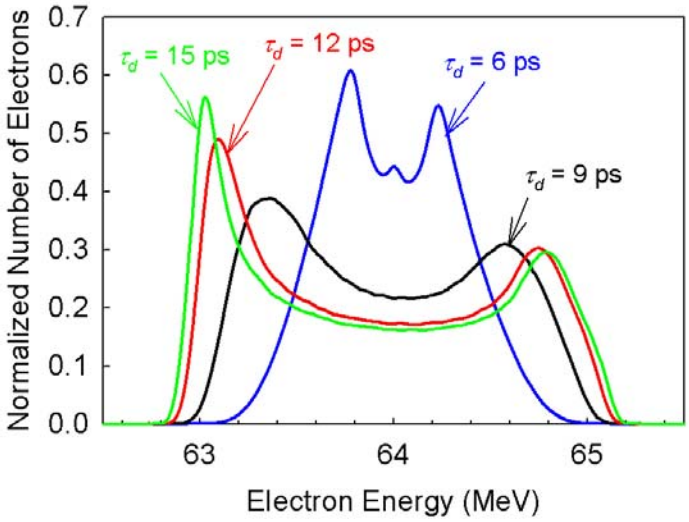

Fig. 2-3. Model prediction for energy spectrum of witness bunch for t_d = 2.97 ps and different time delays between the seed and witness e-beam bunches for an acceleration length L_{acc} = 2 mm.

We see the maximum accelerated witness electrons in Fig. 2-3 gain about 1 MeV over 2 mm corresponding to an acceleration gradient of 500 MeV/m. This was for a laser peak power of 0.5 TW. While this gradient is on the low side compared to typical SM-LWFA devices, it is perfectly acceptable for an LWFA buncher since an energy modulation of order ±1% is only needed. Indeed, if the gradient were too high, it would make it difficult to control the amount of modulation. Nonetheless, a gradient of 500 MeV/m is over 100 times higher than what we obtained using an IFEL.

The seeded SM-LWFA process is certainly capable of reaching acceleration gradients similar to non-seeded SM-LWFA devices. Scaling to longer acceleration lengths is also possible

just as with non-seeded SM-LWFA. For example, for a slightly different configuration, but still assuming only 0.5 TW laser peak power, the model yields an acceleration gradient of 2 GeV/m over a 3 mm distance. Thus, to achieve, say, 100 MeV energy gain would require an acceleration length of 5 cm.

The preceding described the basic approach planned for the seeded SM-LWFA experiment, i.e., the ATF would provide two electron bunches – one to act as the seed bunch to generate the wakefield and the second bunch to act as the witness whose energy spectrum would be measured displaying behavior such as shown in Fig. 2-3. As explained in Sec. 2.4.1, a chicane was used to compress the seed bunch in order to enable generation of the wakefield via PWFA. However, rather than compressing the bunch from the linac, the chicane/dogleg system created two compressed bunches separated in time and energy. Unfortunately, attempts to modify the experiment in order to somehow utilize these compressed bunches were not successful (see Sec. 2.4.2). Therefore, it was decided to create the wakefield using a fast-rising bunch available on an adjacent beamline (Beamline #2). Furthermore, for reasons given later, a witness bunch could no longer be used and coherent Thomson scattering (CTS) was substituted as the means to detect the interaction of the laser beam with the wakefield (see Sec. 2.3.5).

This change in plans required re-exercising the LWFA model to provide predictions for the wakefield strength produced by a fast-rising bunch rather than that generated by an ultrashort bunch, and an estimation for the amount of Stokes and anti-Stokes signal we could expect from the CTS diagnostic. Luckily, Dr. Andreev had already analyzed CTS produced by LWFA [2-15] and he was able to modify his seeded SM-LWFA code to predict the CTS signal for the STELLA-LW conditions. The predictions are described next.

The equations for the *e*-beam and laser beams at the plasma channel entrance are as follows. The laser beam amplitude *a* is given by

$$a(r, z = 0, t) = a_0 \exp\left[-\frac{r^2}{w_0^2} - \frac{(t - t_a)^2}{\tau_{\mathrm{L}}^2} \right], \tag{2-1}$$

wheras the density distribution of the seed bunch was changed from a simple Gaussian shape to one with a fast rise-time as modeled by using a double-Gaussian time shape with different rise τ_{rise} and fall τ_{tail} times, i.e.,

$$n_b(r, z = 0, t < t_b) = n_{b0} \exp\left[-\frac{r^2}{2\sigma_{\mathrm{e}}^2} - \frac{(t - t_b)^2}{2\tau_{\mathrm{rise}}^2} \right], \tag{2-2a}$$

$$n_b(r, z = 0, t > t_b) = n_{b0} \exp\left[-\frac{r^2}{2\sigma_{\mathrm{e}}^2} - \frac{(t - t_b)^2}{2\tau_{\mathrm{tail}}^2} \right], \tag{2-2b}$$

where t_a and t_b determine the delay times between the pulses, $t_d = t_b - t_a$. The radial electron plasma density distribution in the channel is given by

$$n_0(r) = n_0(r = 0)\left[1 + \frac{r^2}{R_{ch}^2} \right], \tag{2-3}$$

where R_{ch} is the radius corresponding to doubling of the on-axis density (see Ref. 2-9).

Table I lists the parameter values used in the model, which were chosen to simulate the parameters anticipated for seeded SM-LWFA experiment performed on Beamline #2. It is assumed the plasma density is uniform along the capillary axis over the entire plasma length with sharp boundaries. [Measurements of the longitudinal plasma uniformity along the 4-mm capillary discharge indicate that the density decreases by a factor of two from the center of the capillary to its ends (see Sec. 2.3.2).] The laser pulse is focused at the capillary entrance ($z = 0$) with time delay t_d = 12 ps. All modeling results were obtained for a dielectric capillary wall with $\varepsilon_{wall} = 2.25$.

Figure 2-4 is the model prediction showing how the plasma density perturbation and the subsequent wakefield potential grows with plasma length. It indicates that the greatest growth occurs after 8 mm. Nonetheless, as shown later, there is sufficient wakefield formation even after 4 mm to generate adequate Stokes and anti-Stokes signals.

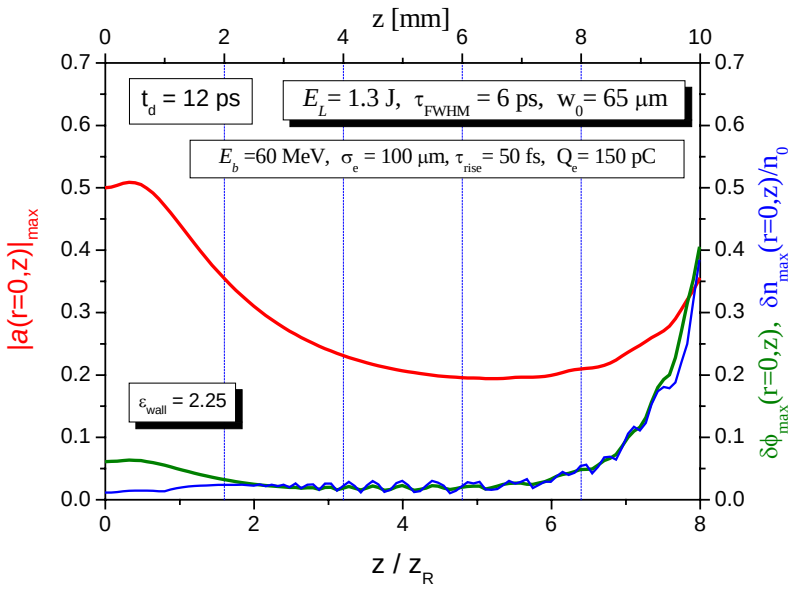

Fig. 2-4. Modeling results using fast-rising seed bunch for plasma density $n_0 = 3.0 \times 10^{17}$ cm^{-3} and laser energy $E_L = 1.3$ J. Plotted are the laser field parameter $|a(r = 0, z)|_{max}$, plasma density modulation in the wake and wakefield potential $\delta\varphi_{max}$ $(r = 0, z)$ as functions of distance along the plasma channel.

Figures 2-5, 2-6, and 2-7 are the model predictions showing how the plasma density perturbation and wakefield potential grows as a function of time after arrival of the fast-rising seed bunch assuming a 4 mm, 8 mm, and 10 mm plasma length, respectively. As the plasma length increases, there occurs a greater amount of self-modulation of the laser field amplitude, which enhances the growth of the wakefield potential. This enhancement represents the amplification of the wakefield due to the seeded SM-LWFA process and is the effect that the experiment was trying to observe.

Table 2-1. Laser and plasma parameters used in seeded SM-LWFA simulations.

Parameters	Value
Laser wavelength, λ_L	10.6 μm
Laser pulse duration, τ_L [(a)]	5.1 ps
Laser peak power, P_L	0.2 TW
Laser pulse energy, E_L	1.3 J
Laser beam focus radius, w_0	65 μm
Laser beam Rayleigh range, z_R	1.25 mm
Normalized laser field strength, a_0	0.762
Plasma length[(b)]	4 - 10 mm
Plasma density on axis, n_0	3.0×10^{17} cm^{-3}
Plasma channel radius R_{ch}	740 μm
Capillary radius R_{cap}	500 μm
P_L/P_{crit} (for relativistic self-focusing)	0.25 and 0.5
Time delay between peak of laser pulse and peak of seed *e*-beam bunch, t_d	12 ps
E-beam energy (seed), E_{inj}	60 MeV
e-beam intrinsic energy chirp [%]	0.5 %[(c)]
e-beam pulse charge	150 pC
e-beam pulse risetime (τ_{rise})	50 fs
e-beam pulse tail length (τ_{tail})	1 ps
Seed *e*-beam focus size at capillary ($1\sigma_e$)[(d)]	100 μm

(a) The full-width-at-half-maximum pulse duration of the laser intensity is equal to $\tau_{FWHM} = \sqrt{2\ln 2}\ \tau_L = 6\,\text{ps}$.

(b) The plasma length is assumed to be the same as the capillary length. Note, during the experiment, the capillary length was 4 mm.

(c) The seed *e*-beam propagates with constant velocity determined by its energy without changing its shape, so the results do not depend on the initial energy spread.

(d) Equivalent to rms.

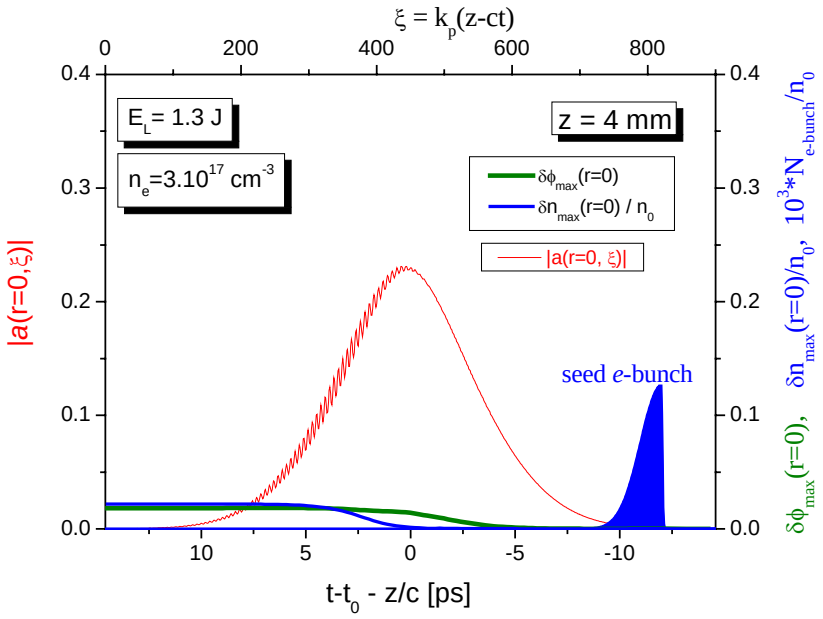

Fig. 2-5. Laser field parameter $|a(r = 0)|$, normalized density variations $\delta n_{max}\ (r = 0)/n_0$ and $\delta\varphi_{max}(r = 0)|$ as functions of time for $z = 4$ mm for the conditions given in Fig. 2-4. Also plotted is the seed e-beam bunch position.

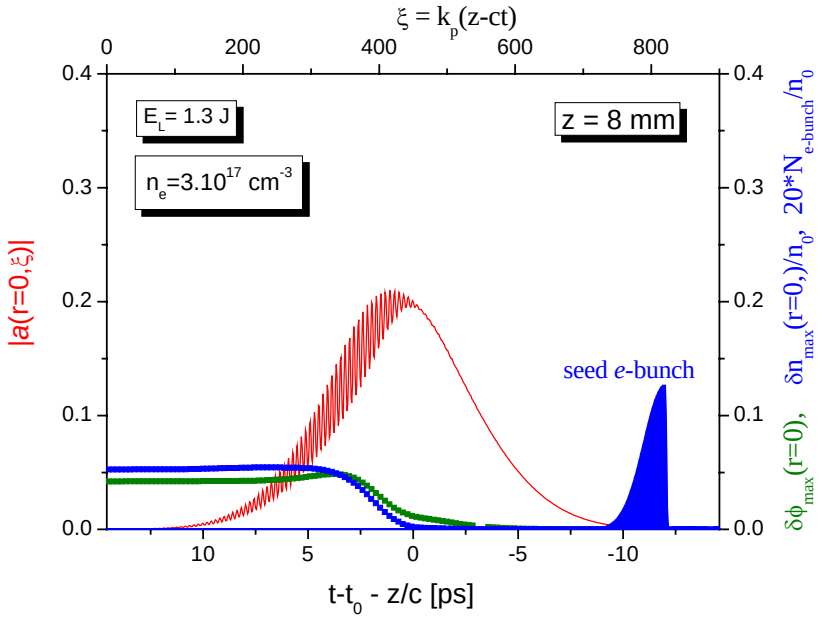

Fig. 2-6. Results for the same conditions as in Fig. 2-5 except the distance of laser propagation $z = 8$ mm, i.e., the plasma length is 8 mm.

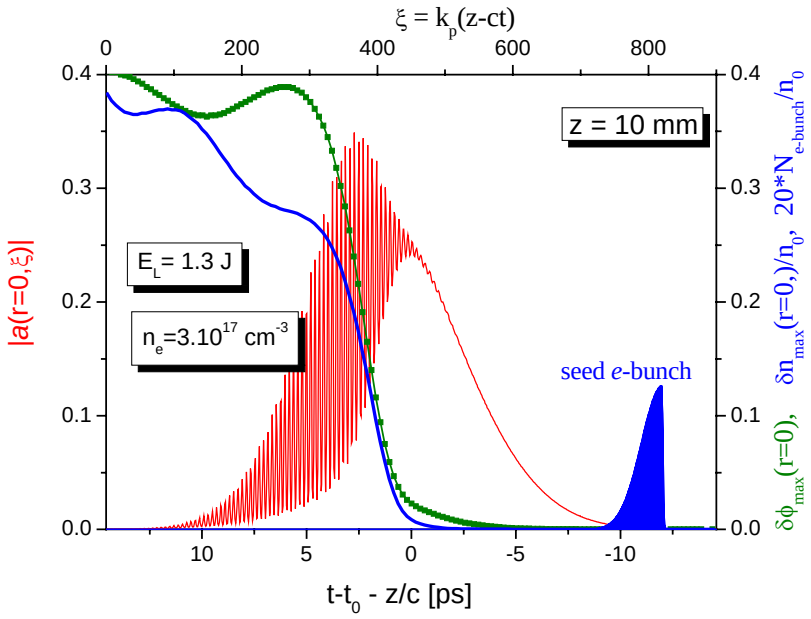

Fig. 2-7. Results for the same conditions as in Fig. 2-5 except the distance of laser propagation z = 10 mm, i.e., the plasma length is 10 mm.

As also can be seen in Figs. 2-6 to 2-7, the tail end of the laser pulse interacts with the wakefield produced by the seed. Not only does this cause amplification of the wakefield, it also means some of the laser photons are scattering off the wakefield. The wakefield acts like a grating and creates higher and lower harmonics (sidebands) of light emission via CTS. The model is able to predict the relative amount of light in the sidebands. Figure 2-8 gives the model predictions for the amount of sideband emission normalized to the fundamental radiation at 10.6 μm for different plasma lengths. Due to the nonlinear growth of the wakefield as a function of plasma length, factors of two changes in the length can cause an order of magnitude change in the sideband signal strength.

Of particular interest are the predictions for z = 4 mm, which is the length of the capillary used during the experiment. We see the predicted Stokes signal is 10^4 to 10^5 times weaker than the fundamental. Since the fundamental has a peak power of order 1 TW, this implies the Stokes signal should be of order 10 MW to 100 MW. This is still many orders of magnitude higher than the minimum sensitivity of the IR detectors used to observe the Stokes emission. Hence, the model indicated that Stokes emission should be readily detectable if the wakefield is present. It should still be observable even if the wakefield is relatively weak due to imperfect conditions.

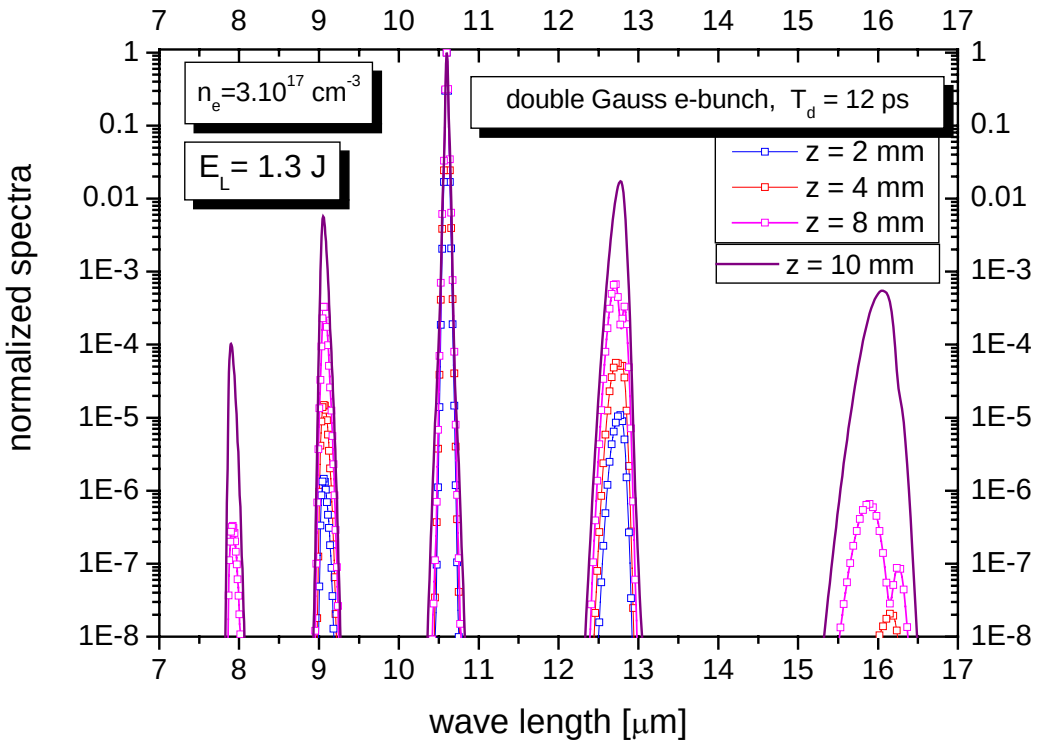

Fig. 2-8. Model prediction for the Stokes and anti-Stokes spectrum produced by the CTS diagnostic. The results are integrated over the radial spectral intensity of the laser pulse after propagating z = 2, 4, 8 and 10 mm.

2.2.2 Pseudo-Resonant LWFA

LWFA experiments typically have been performed using 0.8-1 μm laser wavelengths where TW-level lasers are readily available. The STELLA-LW experiment was to be one of the first to investigate LWFA using 10.6-μm laser wavelength. Wakefield generation at long laser wavelengths has certain inherent advantages [2-16]. One is that the normalized laser field parameter a is proportional to the laser wavelength λ_L (i.e., $a \equiv eE_L/\omega mc$, where e is the electron charge, E_L is the laser electric field, ω is the laser frequency, and m is the electron mass). This means for the same laser beam focus area, 10-μm light will provide a factor of 10 increase in a compared to 1-μm laser light and a 100 times increase in the ponderomotive potential, which scales as a^2. While it is true that 1-μm light can be focused to a smaller area than 10-μm light to compensate for this effect, the minimum usable laser beam size is limited by the minimum *e*-beam size that can be obtained. The *e*-beam size depends on other factors, such as the *e*-beam emittance and space charge spreading. From an experimental viewpoint, larger *e*-beam sizes are generally favored because these limitations are eased. Hence, LWFA at 10.6 μm has certain practical benefits.

Theoretical analysis of LWFA driven by 10.6-μm laser light has already been performed [2-17] - [2-18]. For the final upgraded conditions of the ATF TW CO_2 laser (i.e., ~2 ps pulse length, 5 J/pulse), an electric field gradient of ~1 GV/m is predicted. This is for n_e ~10^{16} cm^{-3},

which is a density higher than the usual density required to satisfy the resonant condition for a 2-ps laser pulse. Even more noteworthy is this high gradient arises from a strong wakefield that is created despite the fact the 2-ps laser pulse is too long for resonant LWFA and too short for SM-LWFA. It was found that interaction of the laser light with the plasma causes pulse steepening to occur at the trailing edge of the light pulse. This effectively initiates the wakefield generation as if the laser pulse length were much shorter, but the pulse terminates before forward Raman scattering (FRS) can play a significant role. Nevertheless, the wakefields produced can be comparable to those formed by SM-LWFA with a longer pulse.

A model simulation [2-9] of the laser pulse steepening effect and subsequent wakefield generation at 5.5 cm into the plasma is shown in Fig. 2-9. Plotted is the laser pulse temporal profile with and without the steepening effect, where the former also displays an increase in height. Plotted is the change in wakefield potential $\delta\Phi = \Phi - 1$, where Φ is the scalar potential of the wakefield normalized by e/mc^2. A significant wake trails after the laser pulse, but the laser pulse terminates before appreciable interaction occurs between the laser pulse and the evolving wake.

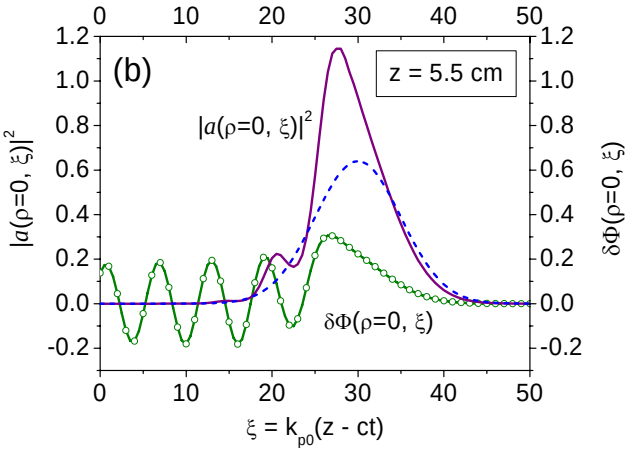

Fig. 2-9. The normalized laser pulse intensity on axis $|a(r=0,\xi)|^2$ *and wakefield potential* $\delta\Phi = \Phi(r=0,\xi) - 1$ *(lines marked by circles) at propagation distances z =5.5 cm.*

We refer to this operating regime as pseudo-resonant LWFA (PR-LWFA) because the laser pulse effectively acts like a shorter pulse that would occur in resonant LWFA. This pulse-steepening phenomenon was also independently uncovered by others [2-19]. Because the laser pulse terminates before significant FRS growth occurs, aspects of SM-LWFA that are difficult to control may be mitigated. Thus the wake produced in the pseudo-resonant regime may be more controllable, which would make it easier to stage the LWFA process.

The preceding model simulation assumed a CO_2 laser peak power of nearly 3 TW at a plasma density of ~10^{16} cm^{-3}. Subsequent modeling analysis indicated that the PR-LWFA effect disappears if one operates at lower peak power even if the plasma density is also reduced. Essentially, at low plasma densities, the laser pulse interacts with the plasma in a linear operating regime and nonlinear pulse steepening effects become negligible. Therefore, demonstration of PR-LWFA at 10.6 μm requires a minimum peak power of 3 TW.

As mentioned, the ATF CO_2 laser is capable of delivering 1 TW pulses. Multi-terawatts is possible, but it requires creation of a 2 ps laser pulse that is amplified to 5 J. Creation of the short CO_2 laser pulse is accomplished using a pulse slicing technique in which a portion of the IR light from the Nd:YAG laser, which drives the ATF photocathode, is used to control the transmission of the CO_2 laser pulse through various optical elements. By this method, arbitrary CO_2 pulse lengths can be sliced out of the longer pulses produced by the CO_2 master oscillator. However, the minimum pulse length that can be sliced out is limited by the rise-time of the Nd:YAG laser pulse.

Figure 2-10 depicts the layout for the ATF CO_2 laser system showing how the 5-J, 5-ps output is generated. The output from the CO_2 master oscillator passes through a preamplifier and then is sliced to a shorter pulse length using the germanium plate switch and Kerr cell. After this the pulse is amplified to 5 J. Note the Nd:YAG laser pulse is 5 ps in duration and its rise-time is too long to slice out a 2 ps CO_2 laser pulse.

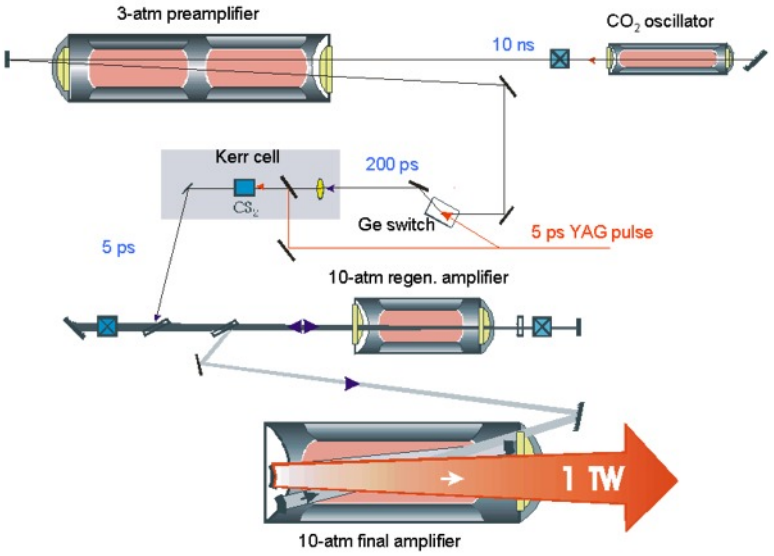

Fig. 2-10. Basic layout for ATF CO_2 laser system.

In 2003 when the STELLA-LW proposal was written, the ATF believed they could achieve a 2-3 ps Nd:YAG pulse for driving the Kerr cell by taking advantage of pulse-shortening during second-harmonic generation (SHG) of the 14-ps long Nd:YAG pulse. This concept was based upon simulations for SHG in crossed-polarized beams, which caused significant pulse shortening compared to the fundamental. At that time, the ATF had not yet experimentally validated this concept nor did they possess an autocorrelator capable of measuring the shorten pulses.

Tests done afterwards revealed that the efficiency of the SHG is not adequate enough to produce sufficient pulse energy for controlling the Kerr-cell switching. Some time later the ATF was able to solve this problem when STI Optronics was able to refurbish and loan the facility a Nd:YAG laser amplifier. This additional amplifier stage is positioned prior to the SHG and produces 10 times stronger SHG (3-4 mJ), which is sufficient for the Kerr-cell switching. By this time, the autocorrelator for SHG had been built and it indicated the shortest pulse that can be achieved is 5-6 ps. This was still a factor of two longer than we require, but it permitted reaching the 1 TW level needed to drive the seeded SM-LWFA experiment.

In order to further shorten the CO_2 laser pulses, the ATF embarked on a new development effort called the Advanced Drive Laser (ADL), in which the entire photocathode laser drive system was to be replaced. It would rely exclusively on direct diode-pumped systems instead of flashlamp-pumped lasers. Efficient 1-μm lasing hosts in a mixed gain media configuration would be used to minimize thermal issues and reduce system size. As part of this major upgrade, an amplifier and optical compressor to enable delivering a 500-fs slicing pulse for the CO_2 laser system would be installed.

It became clear in late 2006 that the ADL upgrade would not be ready by the end of 2007 when the STELLA-LW program was scheduled to end. In fact, it is unlikely the ADL upgrade will be completed in 2008. For this reason the STELLA-LW experiment had no choice but to abandon its effort to demonstrate PR-LWFA and instead focus all work on demonstrating seeded SM-LWFA.

2.3 OVERVIEW OF STELLA-LW EXPERIMENT AND HARDWARE

2.3.1 Description of Experiment Layout

Figure 2-11 shows a schematic layout of the experiment on Beamline #1 at the ATF as it was originally planned. The *e*-beam enters the beamline from the right and is focused into the capillary discharge using various quadrupole magnets. The capillary is housed inside a vacuum chamber, which has input and output windows for the high-power CO_2 laser beam. Various *e*-beam diagnostics are available including beam position monitors (BPM), a coherent transition radiation (CTR) interferometer, and two electron energy spectrometers. One spectrometer has high energy resolution and narrow energy acceptance; the second has less energy resolution, but much larger energy acceptance. The CTR interferometer proved to be an important diagnostic and is described in Sec. 2.3.4.

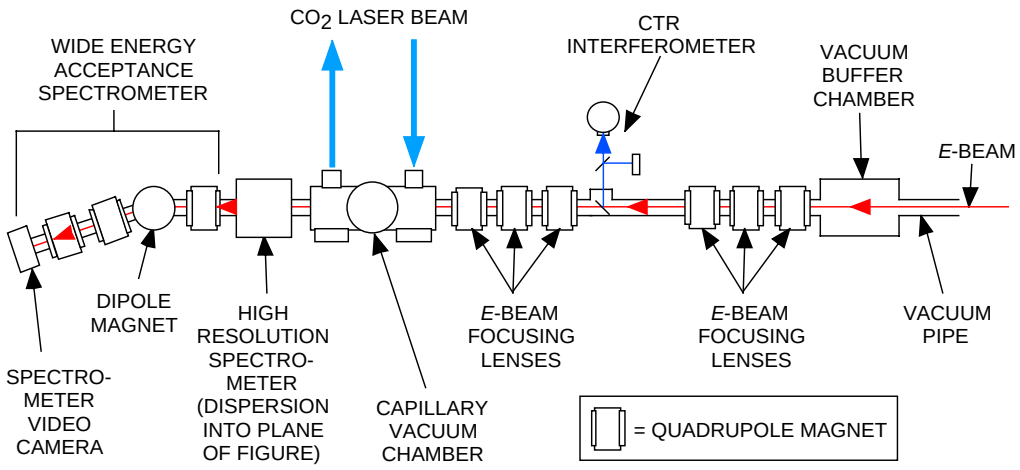

Fig. 2-11. Diagram of STELLA-LW experiment.

Figure 2-12 is a top-view diagram of the capillary vacuum chamber showing the major internal components. A photograph of the vacuum chamber is given in Fig. 2-13.

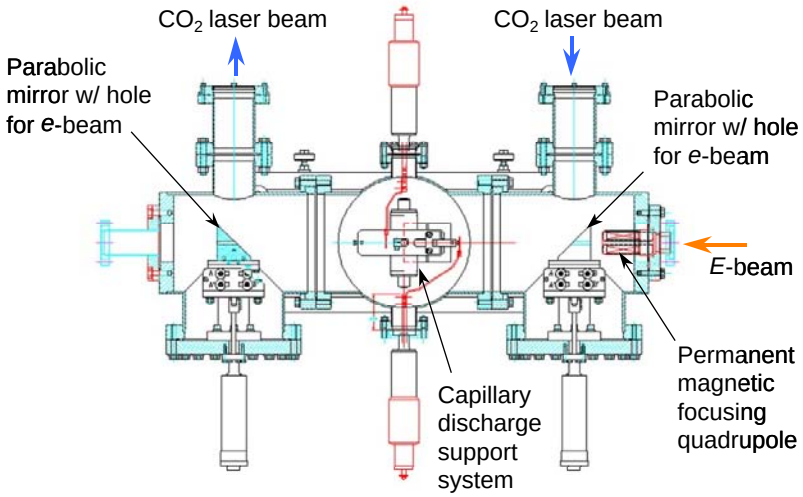

Fig. 2-12. Top-view of capillary vacuum chamber.

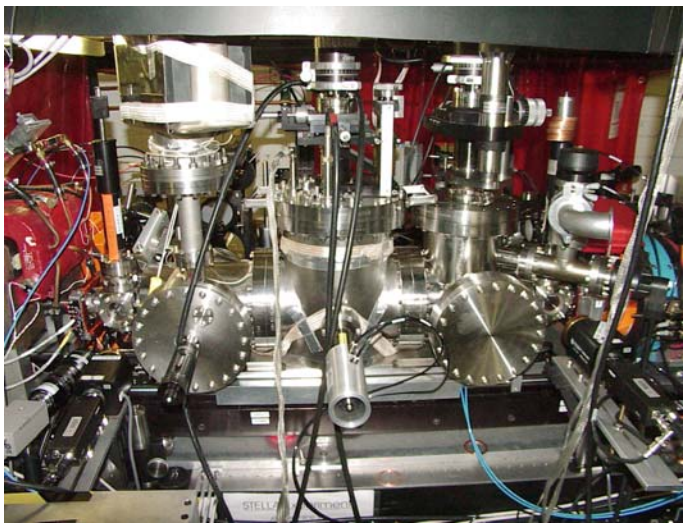

Fig. 2-13. Photograph of capillary vacuum chamber.

2.3.2 Gas-filled Capillary Discharge

During the STELLA-LW program we developed our own gas-filled capillary design basing it upon the pioneering work performed by Dr. Simon Hooker (University of Oxford) and his gas-filled capillaries [2-20]. The basic configuration for our gas-filled capillary is depicted in Fig. 2-14(a). Hydrogen gas is injected in the center of the waveguide, which is 4 mm long and 1 mm diameter. A high-voltage pulse is applied across the electrodes on the ends of the waveguide to ignite the plasma discharge. The hydrogen gas continues to flow out the ends of the capillary into the beamline vacuum.

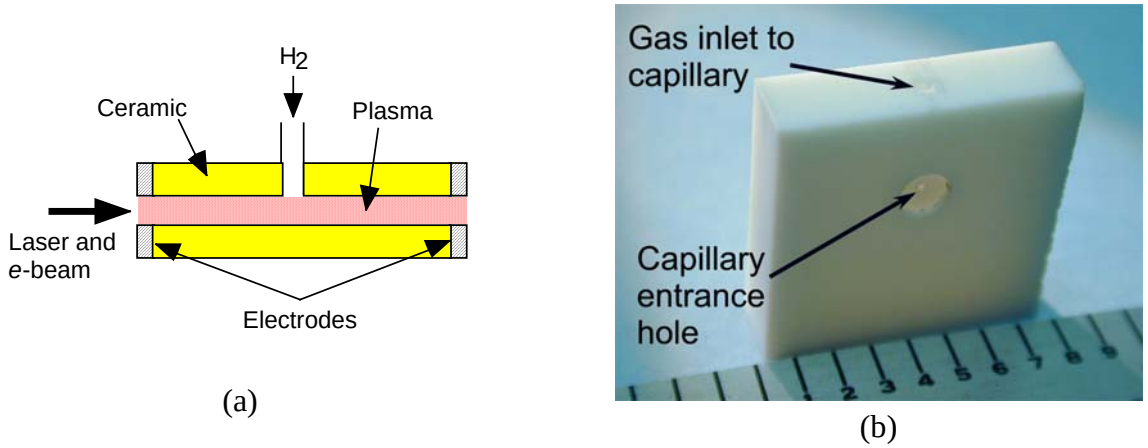

Fig. 2-14. Gas-filled capillary. (a) Schematic of basic gas-filled capillary design used for STELLA-LW. (b) Photograph of Macor™ block fabricated for STELLA-LW showing entrance hole to capillary and side hole for the gas inlet.

Unlike the alumina and sapphire waveguides used by Dr. Hooker, the STELLA-LW gas-filled capillary is constructed from a machinable ceramic called Macor™. This ceramic block is shown in Fig. 2-14(b). Macor™ has dielectric properties similar to alumina and sapphire, and appears to be an acceptable substitute. Macor™ was chosen because it can be easily machined in a conventional machine shop, which greatly facilitates and expedites fabricating and modifying the design of the capillary.

Figure 2-15(a) is a photograph of the assembled gas-filled capillary. Acrylic is used as the mounting fixture for the ceramic block. The electrodes on the ends of the block are offset from each other to discourage tracking along the surface of the ceramic and the plastic mount. Figure 2-15(b) is a cross-sectional, close-up view of the assembled capillary showing how the gas enters the waveguide. This capillary system was designed so that the ceramic block can be easily replaced without changing the mounts. It can also accommodate longer waveguides without modifying the mounts or the electrodes.

A modification to the gas-filled capillary, not shown in Fig. 2-14, are side holes in the Macor block that permit insertion of optical fibers to collect light from along the discharge length. As discussed in Sec. 2.4.3, these fibers were used to collect light for the Stark broadening diagnostic and to determine the longitudinal uniformity of the discharge.

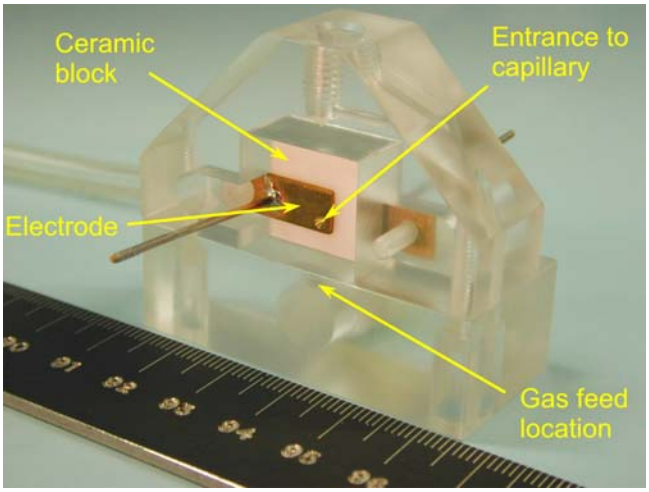

(a)

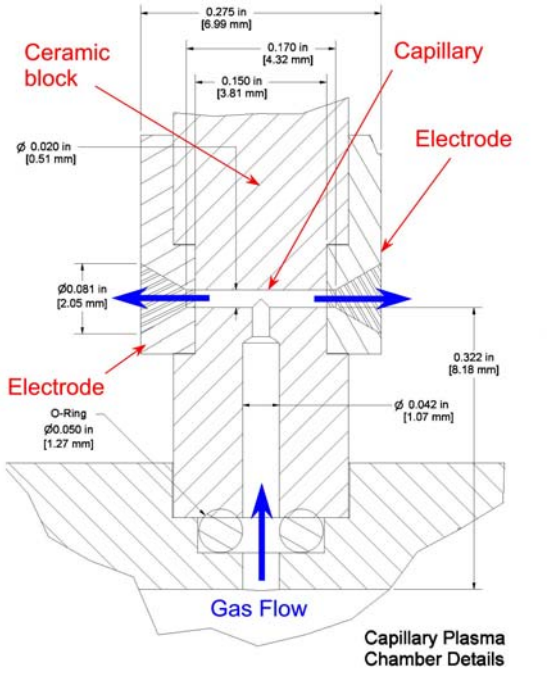

(b)

Fig. 2-15. (a) Photograph of assembled gas-filled capillary showing ceramic block secured to acrylic mounting fixtures. (b) Cross-sectional, close-up view of assembled gas-filled capillary shown in (a).

Also built for the gas-filled capillary was a gas-manifold system for controlling the injection of gas into the capillary. A schematic of the gas-manifold system is depicted in Fig. 2-16. This system uses a gas reservoir, which is preloaded with hydrogen gas. This gas is then released into the capillary using a fast-acting solenoid valve. The valve is a three-way device configured so that in its off-position the capillary inlet gas line is being constantly pumped on by the vacuum system. This helps remove the residual gas inside the capillary when a shot is completed.

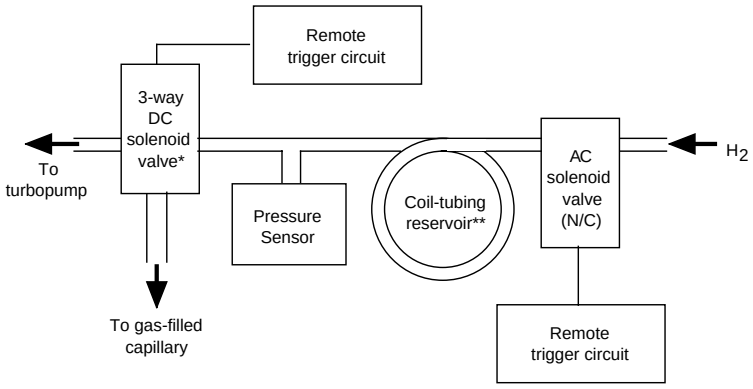

Fig. 2-16. Schematic of gas manifold system for gas-filled capillary.

The low aspect ratio of the length (4 mm) to diameter (1 mm) of the capillary gave rise to concern about the longitudinal uniformity of the plasma. A special capillary was made with three optical fibers positioned along the length of the capillary that allowed sampling the amount

of plasma light emitted along the length of the capillary. The amount of light should be proportional to the plasma density.

Figure 2-17 plots the raw signals from the photodiodes versus position along the capillary at various reservoir pressures. This plot assumes the photodiodes used to detect the light emission transmitted by the fibers have essentially the same sensitivity and there is no significant overlap in the volumes viewed by the fibers. Note that +2 mm and –2 mm represent essentially the ends of the capillary. If the lines plotted in Fig. 2-17 are extrapolated to the ends of the capillary, then we see that the signal drops by ~50% or less. This implies that the plasma density varies along the capillary by a factor of two or less. This amount of variation should be tolerable for our experiment.

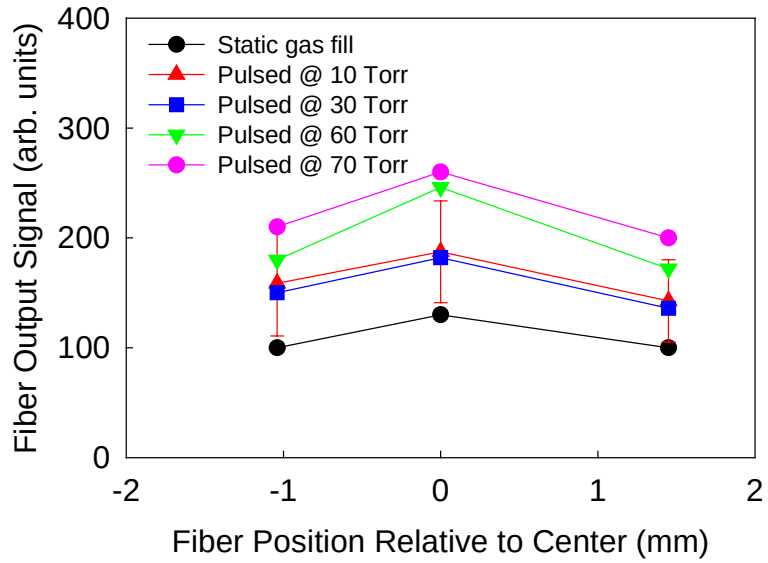

Fig. 2-17. Optical fiber output signal versus position along 4-mm capillary.

2.3.3 Stark Broadening Diagnostic

Knowing the plasma density accurately is a critical aspect of the experiment. Prior gas-filled capillary investigations by Dr. Hooker indicated that near 100% ionization of the gas should be possible [2-20]. However, at low pressures and/or low discharge voltages, the gas may not be fully ionized. Therefore, an independent means for measuring the plasma density was needed.

Fortunately, members of the STELLA-LW team were also collaborating with the multibunch PWFA experiment [2-21] that was also being performed at the ATF. The multibunch PWFA experiment is headed by Prof. Tom Katsouleas and Dr. Patric Muggli from USC. As part of their experiment they developed a Stark broadening diagnostic for directly measuring the plasma density inside the capillary. STI Optronics has helped them develop this diagnostic by providing an image-intensified, fast-gating camera for observing time-resolved spectral emissions from the capillary. The STELLA-LW program also shared our gas-filled capillary for their usage.

Stark broadening of the hydrogen Balmer α-line at 656 nm and the Balmer β-line at 486 nm is a well-known function of the electron density and temperature [2-22], with the Hβ line being less sensitive to the electron temperature than the Hα line. Light emission from one end of

the capillary is relay-imaged onto the end of an optical fiber. The other end of the fiber sends the light into a spectrometer and the fast-gating camera as shown in the photograph in Fig. 2-18. More details of the Stark broadening diagnostic can be found in [2-23].

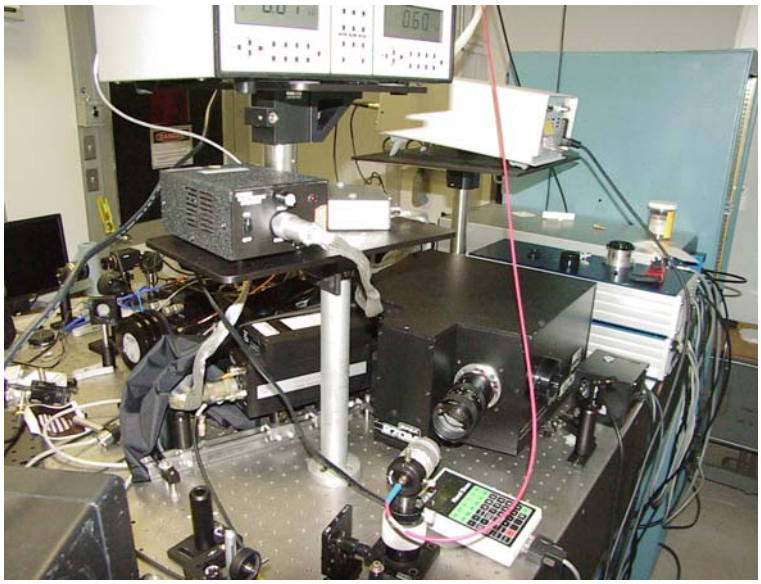

Fig. 2-18. Photograph of optical fiber (red cable in photo) from capillary being coupled into the spectrometer (black box). To the left of the spectrometer oriented at an angle with respect to the spectrometer box is the fast-gated camera on loan from STI Optronics.

Using the fine grating and no gating of the fast-gating camera (i.e., time-integrated mode), the $H\alpha$-line spectrum of the gas-filled capillary was measured as a function of reservoir gas pressure and charge voltage. Bekefi's book [2-22] has tabulated Stark broadening data that gives electron density versus linewidth $\Delta\lambda$ for various hydrogen lines. The plot for the $H\alpha$-line at 40,000 °K is replotted in Fig. 2-19. Using a least-squares curve fitting routine, it is possible to find a very good fit (R = 0.99999192) to this data. This curve fit is also plotted in Fig. 2-19.

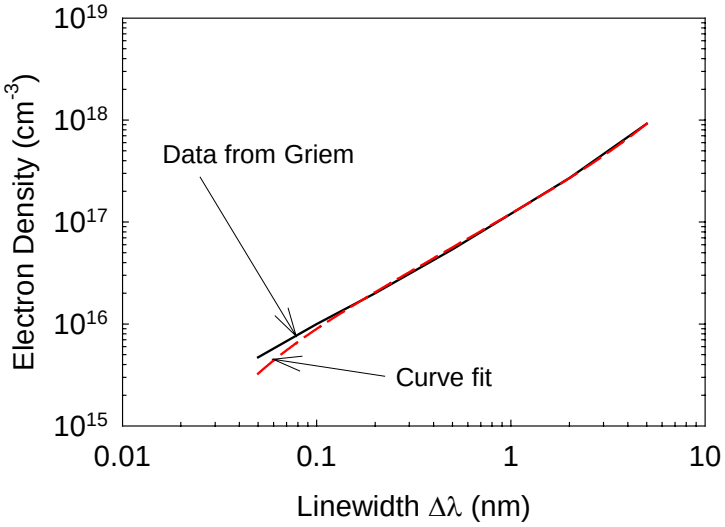

Fig. 2-19. Electron density versus Stark broadened linewidth from Ref. [2-22] and the curve fit [Eq. (2-4)] to the data.

The equation for the curve fit is given below.

$$n_e = 6.05\times10^{17}\, e^{0.185\Delta\lambda} - 6.07\times10^{17}\ \text{cm}^{-3} \qquad (2\text{-}4)$$

The difference between the curve fit equation and the data in Fig. 2-19 is only a few percent over the range 10^{16} to 10^{17} cm^{-3}. In the 10^{17} cm^{-3} range, the difference is less than 1%. Thus, Eq. (2-4) was used to estimate the plasma density under the assumption that temperature affects are not significant.

The raw spectrum images from the spectrometer camera have data in half-frames with typically only one half-frame containing the majority of the signal. An example of a raw video image (negative video image) is shown in Fig. 2-20(a). The raster lines of the appropriate half-frame (100 lines) are extracted from the image and averaged together by adding all the pixel values in each column. The resulting line profile is given in Fig. 2-20(b)

(a)

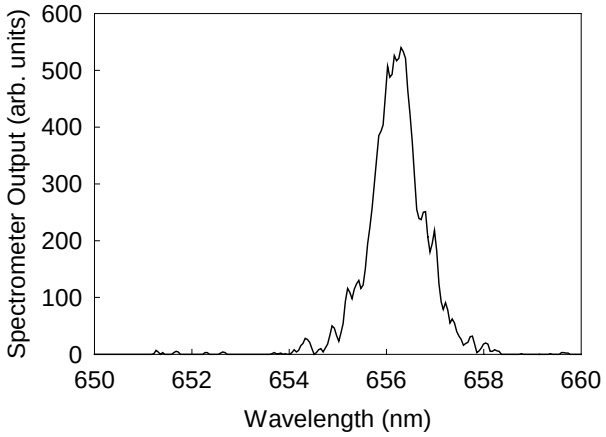

(b)

Fig. 2-20. (a) Example of raw video image from spectrometer camera. (b) Line profile of image shown in (a) after averaging over 100 raster lines.

The wavelength dispersion calibration of the images is determined by measuring the spectrum from a mercury pen lamp. This yielded a dispersion factor of 0.0458 nm/pixel. Absolute wavelength calibration is made by setting the peak of the $H\alpha$-line to 656.3 nm.

The linewidth is measured at full-width-half-maximum for each line profile spectrum and then Eq. (2-4) is used to calculate the plasma density. The results are plotted in Fig. 2-21 where the error bars represent the variance of the density within each set of data.

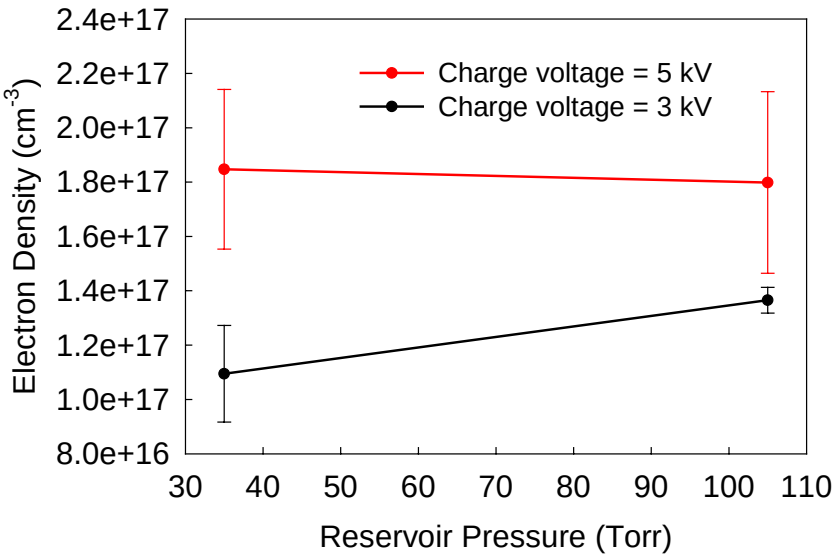

Fig. 2-21. Plasma density results inside the capillary as a function of the reservoir pressure.

At 35 Torr and 3 kV charge voltage, the plasma density appears to be close to 1×10^{17} cm^{-3}. When the pressure in the reservoir is increased by 3 times to 105 Torr, the plasma density only increases by ~30%. This may indicate incomplete ionization of the gas. This is consistent with the 5-kV data, which all display higher plasma densities for the same gas pressures. However, the 5 kV data also displays little dependence on the reservoir pressure, which seems to imply that some other process is controlling or affecting the linewidth. Based upon this result it was apparent the best way to adjust the plasma density would be to monitor the energy loss of the seed bunch as a function of gas pressure.

2.3.4 Coherent Transition Radiation (CTR) Interferometer Diagnostic

A coherent transition radiation (CTR) interferometer was used to characterize the ATF compressed *e*-beam. For the *e*-beam bunches of interest to STELLA-LW, the CTR light is at THz frequencies. Figure 2-22 shows a schematic diagram of the CTR interferometer system. The Michaelson interferometer part of the system, which consists of a beamsplitter and a fixed and translating mirror designed for THz radiation, is a commercial device [2-24]. For our experiments, its operation was modified by foregoing usage of a reference detector since the ATF only had one detector highly sensitive to THz radiation (liquid-helium-cooled bolometer).

By scanning the translation mirror shown in Fig. 2-22, the autocorrelation of the CTR signal is obtained. Analysis of this autocorrelation signal yields information about the *e*-beam bunch characteristics [2-25]. Figure 2-23 shows two examples of the autocorrelation data and the curve fits derived from the autocorrelation integrals for the case of a single and double *e*-beam bunch(es).

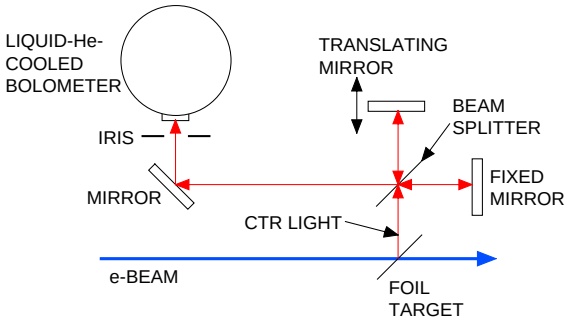

Fig. 2-22. Schematic diagram of CTR interferometer.

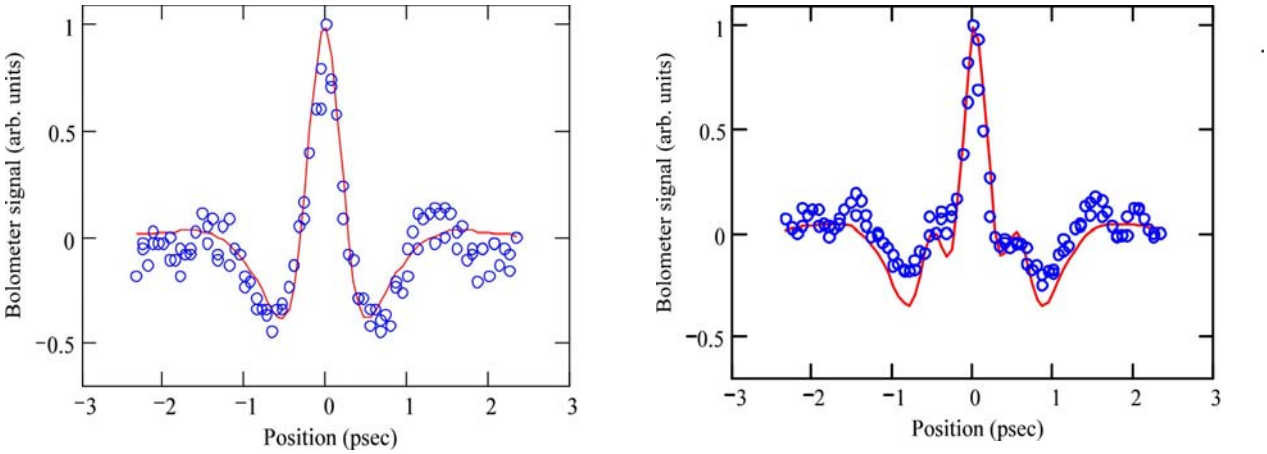

(a) (b)

Fig. 2-23. Example of raw data from CTR interferometer (blue circles) and the curve fits to the data (red line) calculated from the autocorrelation integral [2-25]. (a) Single e-beam bunch. (b) Double e-beam bunches.

For a single bunch, the curve fit of the autocorrelation integral with the data requires selecting values for the bunch length and the cut-off frequency of the detection system.[1] In particular, the width of the central peak of the autocorrelation signal is primarily affected by the bunch length. The shape of the curve on either side of the peak is mostly affected by the cut-off frequency. For the curve fit shown in Fig. 2-23(a), we find the bunch length is 144 fs and the cut-off frequency is 1.7 THz.

For a double *e*-beam bunch, which will be discussed in more detail in Sec. 2.4.1, there are five free parameters in the autocorrelation integral. Using CTR and BPM data for each bunch of the double bunches permits reducing the number of free parameters to two, i.e., the time delay between the two bunches and the cut-off frequency. For the case of the data shown in Fig. 2-23, the single-bunch CTR data indicates the lengths of the two bunches is 144 and 90 fs, and the BPM data indicates the second bunch had ~60% of the charge in the first bunch. Hence, for the curve fit shown in Fig. 2-23(b), we find the time delay between the bunches is 500 fs and the cut-off frequency is 1.8 THz.

[1] A Gaussian-shaped *e*-beam bunch profile is assumed.

2.3.5 Coherent Thomson Scattering (CTS) Diagnostic

Coherent Thomson scattering (CTS) has been used extensively to diagnose the wakefields produced in plasmas [2-26], [2-27]. Briefly, in CTS, the wakefield creates a density perturbation in the plasma that acts like a grating to laser light traveling through the plasma. This light coherently scatters off the wakefield producing sideband light at frequencies ω_S given by $\omega_S = \omega_L \pm \omega_p$, where ω_L is the laser beam frequency and ω_p is the plasma frequency. Hence, the existence of light emission at these sideband frequencies is indirect evidence that the wakefield exists. Moreover, the magnitude of the sideband signal is proportional to the depth of the wakefield. Therefore, comparing the relative strength of the sideband signal gives an indication of the strength of the wakefield potential. These attributes of CTS would permit us to indirectly measure the wakefield characteristics during seeded SM-LWFA and, in particular, to hopefully observe amplification of the wakefield when the laser beam is present.

For the seeded SM-LWFA experiment, the nominal plasma density is $n_e \sim 1 \times 10^{17}$ cm^{-3} assuming a seed bunch length of order 100 fs. However, for the fast-rising seed bunch, the optimum plasma density is $n_e \sim 3 \times 10^{17}$ cm^{-3}. The corresponding plasma frequency can be calculated using the formula given by

$$\omega_p(\text{rad/sec}) = 5.64 \times 10^4 \sqrt{n_e(\text{cm}^{-3})}\,. \tag{2-5}$$

Substituting 3×10^{17} cm^{-3} into Eq. (2-5) we obtain $\omega_p = 3.09 \times 10^{13}$ rad/sec. The CO_2 laser wavelength of $\lambda_L = 10.6$ μm corresponds to a frequency of $\omega_L = 2\pi c/\lambda_L = 1.78 \times 10^{14}$ rad/sec.

The Stokes frequency is calculated by $\omega_S = \omega_L - \omega_p = 1.47 \times 10^{14}$ rad/sec. Converting to wavelength, we therefore find the Stokes wavelength will be

$$\lambda_S = \frac{2\pi c}{\omega_S} = 12.8\mu m\,. \tag{2-6}$$

The anti-Stokes frequency is given by $\omega_{AS} = \omega_L + \omega_p = 2.09 \times 10^{14}$ rad/sec. Converting to wavelength, we obtain

$$\lambda_{AS} = \frac{2\pi c}{\omega_{AS}} = 9.02\mu m\,. \tag{2-7}$$

The preceding Stokes and anti-Stokes wavelengths are for a specific plasma density assuming a certain characteristic of the seed bunch. In reality, the actual plasma density during the experiment must be adjusted to maximize the wakefield produced by the seed bunch and this density would not be necessarily at 3×10^{17} cm^{-3}. Therefore, Fig. 2-24 shows how the Stokes and anti-Stokes wavelengths vary with plasma density. If the fast-rising seed bunch a slower or faster risetime than 50 fs, then the resonant plasma density will be lower or higher than 3×10^{17} cm^{-3}, and the corresponding sideband wavelengths will be shifted as shown in Fig. 2-24.

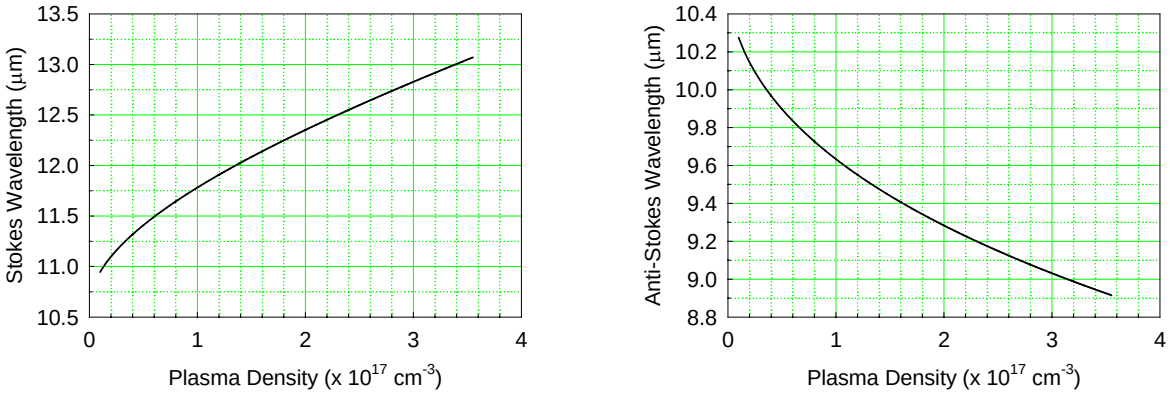

(a) (b)

Fig. 2-24. CTS sideband wavelengths as a function of plasma density. (a) Stokes wavelength. (b) Anti-Stokes wavelength.

Figure 2-25 shows the basic layout for the CTS diagnostic system. The TW ATF CO_2 laser beam enters and exits the capillary vacuum chamber through a pair of windows (the chamber outline is not shown in Fig. 2-25). An off-axis parabolic mirror (f = 10 in = 25.4 cm) focuses the beam into the capillary and an identical off-axis parabolic exit mirror recollimates the laser light. The laser light, which includes both the fundamental and any sideband radiation, is directed to a grating using a pair of mirrors. A 2.5"-diameter positive lens (f = 9 in = 22.9 cm) collects the Stokes or the anti-Stokes light and focuses it into the detector. An optical filter in front of the detector helps block out the fundamental light. Observing the higher-order light of a HeNe laser beam scattered off the grating made it is possible to estimate the proper position of the IR detectors for sensing a particular wavelength.

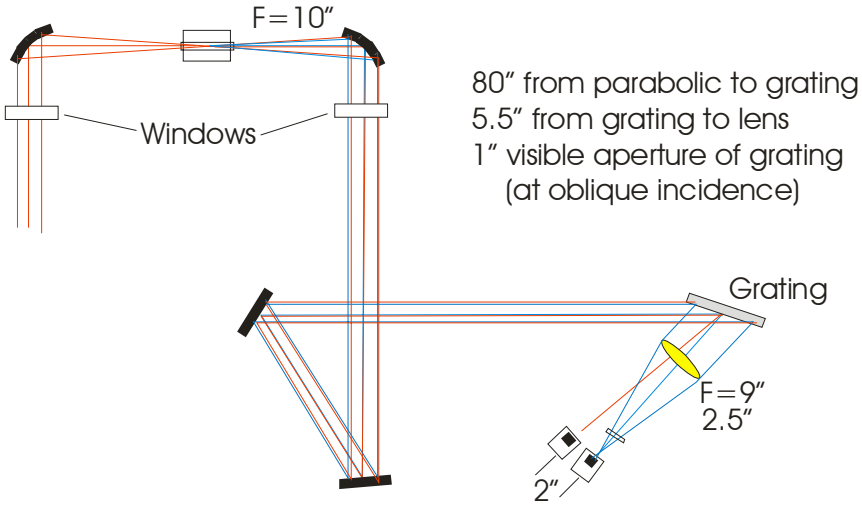

Fig. 2-25. Basic layout for CTS diagnostic system. During the actual seeded SM-LWFA experiment the distances of separation changed from those shown in this figure.

During testing of the CTS diagnostic it was discovered that the ATF TW CO_2 laser beam emits strong parasitic radiation at wavelengths near 9 μm. This parasitic radiation not only interferes with distinguishing the anti-Stokes signal near 9 μm, the radiation is also intense enough to damage the detector. Therefore, the CTS diagnostic was realigned to detect the Stokes emission at around 12.8 μm where there was no parasitic radiation.

The primary IR detector was a pyroelectric 2-D detector array (Pyrocam-III made by Spricon). The Pyrocam-III under pulsed operation has a sensitivity (peak noise limit) of 7 nJ/pixel or 70 μJ/cm^2. The active area of the detector array is 12.4 mm × 12.4 mm = 1.53 cm^2. Its saturation fluence is 10 mJ/cm^2 and its damage threshold is 20 mJ/cm^2 (1 ns pulse).

For the CTS diagnostic, the measured dispersion of the grating (75 grooves/mm) was 0.054 μm/mm. The Pyrocam-III was positioned so that the center of the detector array was aligned to 12.8 μm. This meant for its 12.4 mm array width and the aforementioned dispersion that the Pyrocam-III was able to view emission from 12.1 μm to 13.5 μm. This covered a corresponding plasma density range of 1.6×10^{17} cm^{-3} to 4.6×10^{17} cm^{-3}. Hence, this meant we would be able to detect the Stokes emission over a fairly wide plasma density range. This gave us the freedom to vary the plasma density in order to optimize the wakefield formation by the seed bunch without fear of losing the ability to detect the Stokes emission.

As mentioned, the model simulation for the CTS signal predicted a peak power for the Stokes emission of 10 MW to 100 MW. For a 5-ps laser pulse, this corresponds to 50 μJ to 500 μJ of pulse energy. To account for imperfect conditions, we can degrade the lowest value by a factor of 10, i.e., assume that 5 μJ of Stokes light is produced. The emitted Stokes light will follow a similar divergence as the fundamental laser beam. Thus, the size of the Stokes beam at the detector position should be similar to the fundamental beam size. We allowed some of the fundamental light to be sensed by the Pyrocam-III camera and the resultant image is shown in Fig. 2-26. Since the active area corresponds to 12.4 mm × 12.4 mm, this indicates that the area of the fundamental beam on the detector is roughly 6×10^{-3} cm^2. Assuming this area size for the Stokes beam and 5 μJ of Stokes light, we obtain a fluence on the detector of 0.8 mJ/cm^2. This is an order of magnitude greater than the minimum sensitivity of the Pyrocam-III. Hence, this implies an order of magnitude additional sensitivity margin in our detection capability.

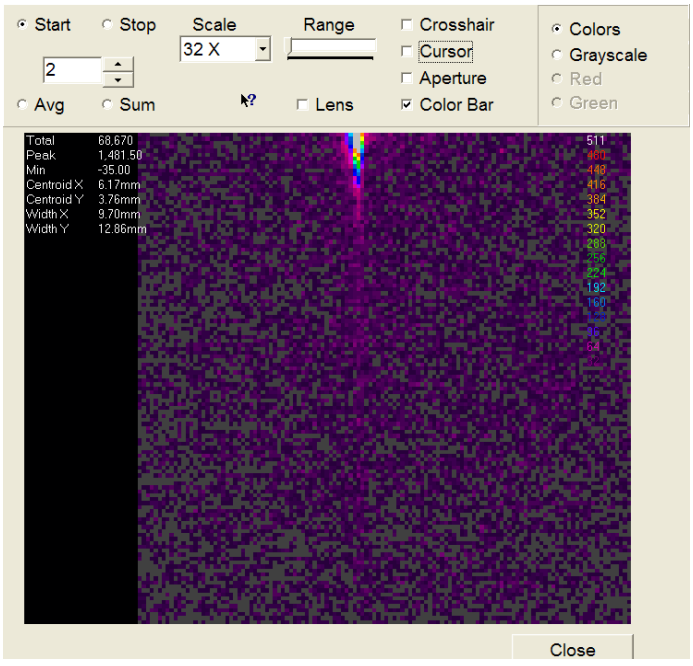

Fig. 2-26. Example of image obtained by Pyrocam-III IR camera of the fundamental laser beam at 10.6 μm located at the top-center of the frame..

Allowing the fundamental beam to be captured by the Pyrocam-III camera also verified that our timing was correct for detecting any Stokes emission. Thus, the relatively high

sensitivity of the camera and its broad wavelength acceptance range ensured that the CTR detector system was capable of sensing the Stokes radiation.

2.4 EXPERIMENTAL RESULTS FOR SEEDED SM-LWFA EXPERIMENT

2.4.1 Formation of Double-Bunch Seed Beam

A chicane designed by UCLA [2-29] was installed on the ATF linac. It was designed to provide approximately 30 times compression and initial model predictions indicated this should be sufficient to produce a ~100 fs bunch for the seeded SM-LWFA experiment. However, there is no acceleration section downstream of the chicane that could be used to compensate for the energy chirp imparted on the beam entering the chicane. Instead, it was thought that coherent synchrotron radiation (CSR) could fulfill this role.

As mentioned earlier, when the chicane compresses the *e*-beam pulse it creates two ~100 fs bunches separated in time and energy. Our hypothesis is that the double-bunch formation is caused by the interaction between the chicane and the dogleg dipoles downstream of the chicane that direct the *e*-beam into Beamline #1. Figure 2-27 is a cartoon illustrating one possible explanation for the double-bunch formation process. Drawn in blue is the pathway taken by the *e*-beam as it travels through the chicane and dogleg dipoles. Dipoles are indicated as rectangles. Ideally, the *e*-beam enters the chicane with a linear energy chirp as depicted by the dashed line in the energy-time graph drawn in the upper left-hand corner of Fig. 2-27. In reality, we believe the chirp is curved as shown in the graph. It is possible to identify two regions on this curve – Region 1, corresponding to electrons with a high amount of chirp, and Region 2, corresponding to electrons with a small amount of chirp. Note the Region 1 electrons precede the Region 2 electrons.

In passing through the first two dipoles of the chicane, electrons in Region 2 become compressed (we shall refer to these electrons as Bunch 2) and the electrons in Region 1 are not compressed yet (we shall call these electrons Bunch 1). In this middle section of the chicane, the beam is wide and, therefore, CSR is weak. However, between the third and fourth chicane dipoles, the focus is tight and Bunch 1 experiences strong CSR effects. Consequently, after passing through the last dipole of the chicane, the Bunch 1 electrons finally are compressed, but now the Bunch 2 electrons become overcompressed. And, in the process of being overcompressed, the Bunch 2 electrons overtake in time the Bunch 1 electrons (see energy-time graph in middle-top of Fig. 2-27). Finally, the electrons pass through the dogleg dipoles where the beam is nominally focused to a tight spot. Now the strong CSR works on the Bunch 2 electrons to reduce their energy spread. The net result is a clean separation in energy and time between Bunches 1 and 2 as illustrated in the energy-time graph in the lower right-hand corner of Fig. 2-27.

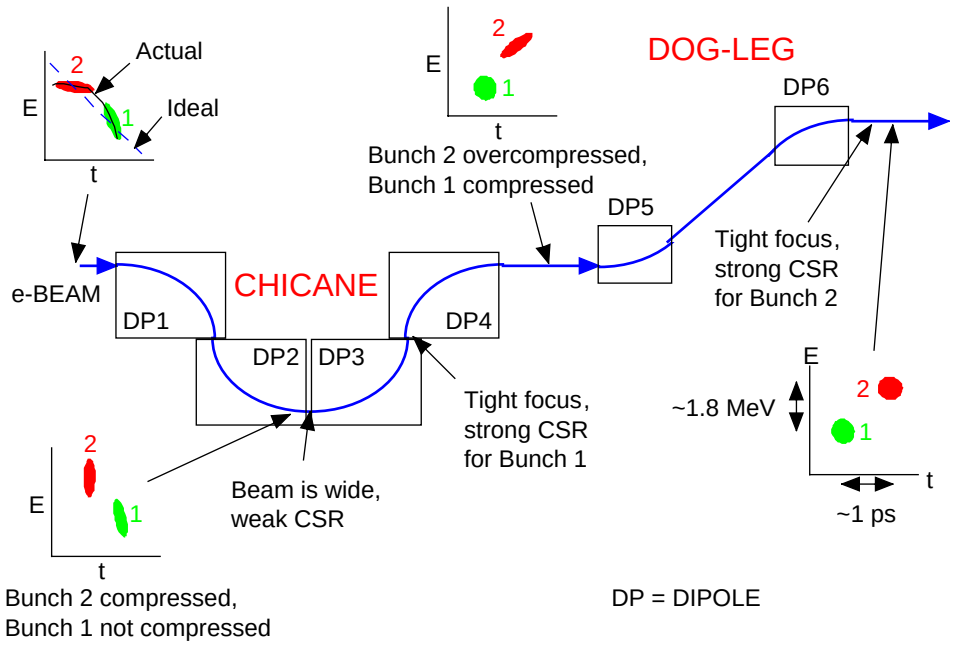

Table 2-27. Cartoon of chicane/dogleg system showing a possible scenario for the double-bunch formation process.

Figure 2-28 are energy spectrums of the *e*-beam at different positions along the pathway depicted in Fig. 2-27. Figure 2-28(a) is just before the chicane. The *e*-beam is a single bunch with an energy width of ~4% FWHM. Figure 2-28(b) is at the high-energy slit located downstream of the chicane. It shows two distinct beams with, in this particular case, most of the charge in the lower-energy bunch (energy dispersion increases to the left in the images). Figure 2-28(c) is at the spectrometer at the end of Beamline #1. The two bunches are separated by approximately 1.8 MeV [see Fig. 2-30(a)]

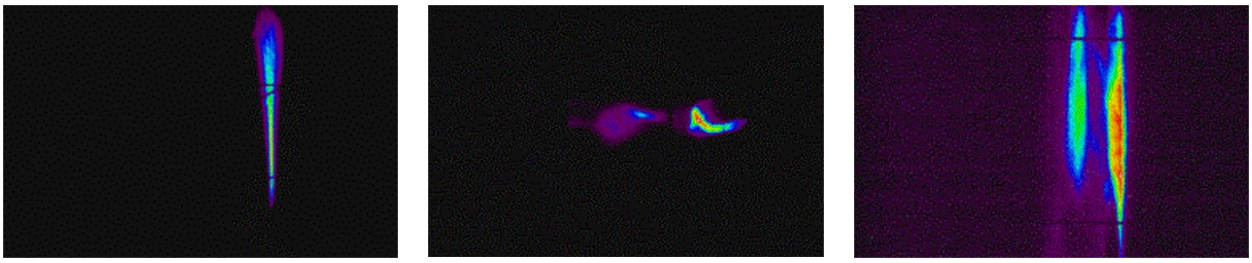

(a) *(b)* *(c)*

Fig. 2-28. Energy spectrums of double-bunch e-beam. Energy dispersion increases to the left. (a) Before the chicane and without compression. Energy spread is ~4% FWHM. (b) At the high-energy slit located downstream of the chicane. (c) At the spectrometer at the end of Beamline #1.

We should emphasize that the preceding explanation is only a conjecture. Initial modeling of the chicane/dogleg system was done using ELEGANT. Preliminary results of this analysis are given in Fig. 2-29. Figure 2-29(a) shows an example of the beam entering the chicane with a curved energy chirp. Figure 2-29(b) gives the resultant energy-time distribution of the electrons after the dogleg. It is clear there has been a separation in energy of the electrons

with a large group congregated in the lower half of the plot and a smaller group in the upper half. ELEGANT also indicates this separation in energy does not occur if CSR effects are turned off in the model. The modeling effort was not continued when it became apparent that ELEGANT is not capable of fully modeling all the physics occurring in the chicane-dogleg system, such as space charge effects. It is not clear that any model exists yet that incorporates all the needed physics.

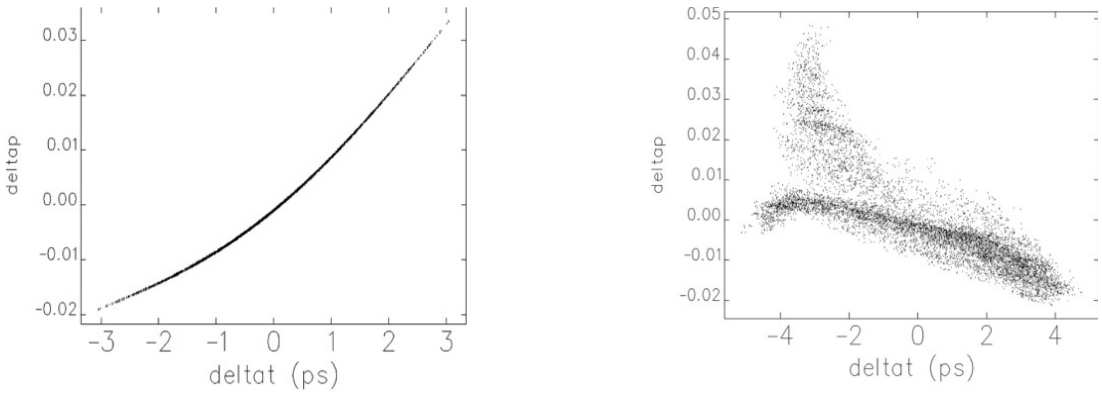

Fig. 2-29. Examples of output plots from ELEGANT of the chicane/dogleg system. (a) Momentum-time plot of electrons entering chicane. (b) Momentum-time plot of electrons at exit of dogleg.

2.4.2 Experimental Results Related to Double-Bunch *E*-Beam

In order to determine whether the double-bunch *e*-beam could be used for the seeded SM-LWFA experiment, a series of runs were performed to better understand the new phenomenon and characterize the beam. Figure 2-30 shows energy spectrums of the double-bunch beam measured by the Beamline #1 spectrometer. Figure 2-30(a) is a single shot showing the two bunches separated in energy by 1.8 MeV. For the sake of identification we have labeled one bunch as the "high-energy (high-E) seed" and the other bunch as the "low-energy (low-E) seed." Figure 2-30(b) is an overlay of three shots taken many minutes apart. We see good reproducibility of the spectrums indicating the energy distribution and positions are stable. However, subsequent runs also showed it is very difficult to obtain the same characteristics of the double-bunches from one run to another. In other words, the pulse widths and energy spectrums were different for each run probably because a complex series of steps are needed to tune the linac to create the double-bunches.

Next, the double-bunches were characterized using the CTR interferometer diagnostic. Since the bunches are separated in energy by about 1.8 MeV, it possible to block one of the bunches from reaching the spectrometer on Beamline #1 by using the variable high-energy slit located downstream of the chicane [see Fig. 2-28(b)]. This allowed CTR interferometer measurements to be taken individually on each bunch. These indicated that the two bunches have comparable bunch lengths of order 100-200 fs and they are separated in time by 0.5-1 ps. But, the CTR interferometer measurements could not tell us which bunch came first.

The amount of charge in each bunch can be measured using either a Faraday cup or by integrating the intensity of each bunch image seen on a BPM [e.g., Fig. 2-28(b)]. Depending on the *e*-beam tune through the chicane and dogleg, the bunches can have comparable amounts of

charge or very different amounts. As discussed later, it turns out the amount of charge in each bunch affects the wakefield interference between the bunches.

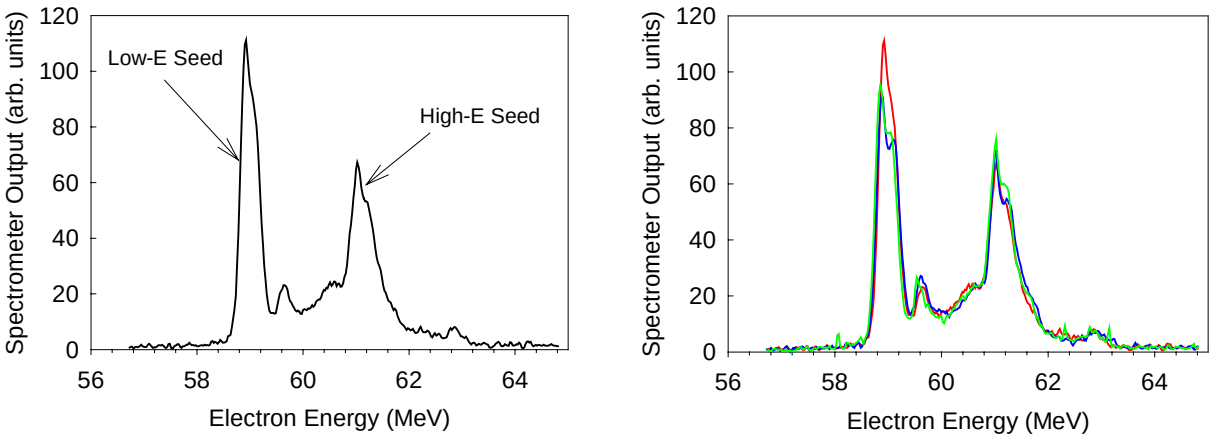

Fig. 2-30. Energy spectrums of double-bunch e-beam. (a) Typical single shot spectrum for the case when both bunches have comparable charge. (b) Three spectrums taken many minutes apart demonstrating stability of the double-bunch formation process.

The seeded SM-LWFA experiment needed a wakefield that can be amplified by the laser pulse. In principle, it did not matter whether this wakefield is created by a single seed bunch or two bunches. Therefore, a key question was does the double-bunch beam still produce wakefields and, if so, how might they be utilized to perform the seeded SM-LWFA experiment? To attempt to answer this question, the double-bunch beam was sent through a polypropylene capillary.

Each of the ~100-fs long seed bunches is capable of generating wakefields. In doing so the electrons must lose energy. Moreover, this energy loss should be a function of the plasma density since for a given bunch length there is a specific plasma density for optimum wakefield generation. Figure 2-31 shows the energy loss of the high-energy and low-energy seed bunches as a function of delay time with respect to the onset of the capillary discharge current. The delay time is plotted increasing to the left so that the plasma density increases to the right in the figure. We see when both bunches propagate through the plasma, the high energy seed (red dots) monotonically loses more energy with increasing plasma density. However, this is not true for the low-energy bunch (blue triangles). The energy loss of the low-energy bunch first increases with higher plasma density, then decreases to a low point at 1 μs delay time. (Due to disruption by the discharge current pulse, data could not be reliably taken for delay times less than 1 μs.) If the low-energy seed is sent through the plasma by itself (black squares in Fig. 2-31), then it also exhibits the same monotonic energy loss with increasing plasma density as the high-energy seed. In fact, the loss rate is essentially the same for both seeds when they travel alone through the plasma. This is strong evidence that the high-energy seed must precede the low energy seed because the presence of the high-energy seed appears to be affecting the low energy seed. Indeed, as the modeling will show below, the wakefields produced by the high-energy seed can interfere with the wakefields produced by the low-energy seed.

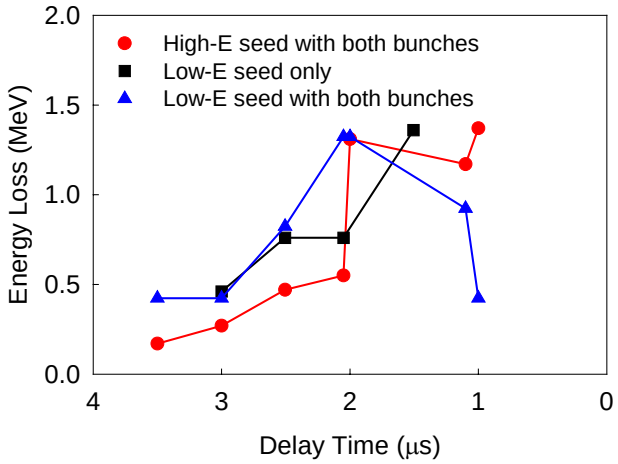

Fig. 2-31. Energy loss data for the double-bunch beam passing through a polypropylene capillary

One tremendous benefit with our collaboration with the multibunch PWFA experiment is the ability to use their codes for modeling the wakefield formation process of multiple electron bunches. These models were developed to study how a train of microbunches can enhance the PWFA process. They work equally well if you only have two bunches.

USC graduate student, Efthymios (Themos) Kallos, ran a 1-D PIC code to simulate wakefield formation assuming the parameters for our double-bunch beam. Figure 2-32 shows an example of the predicted wakefield evolution produced by the double bunches at a specific plasma density (5×10^{16} cm^{-3}). The dark curve shows the two bunches with the leading bunch having an energy of 61 MeV and the trailing bunch having an energy of 59 MeV. Not evident from the wakefield plot is that the wakefield is actually a combined one with contributions from each bunch.

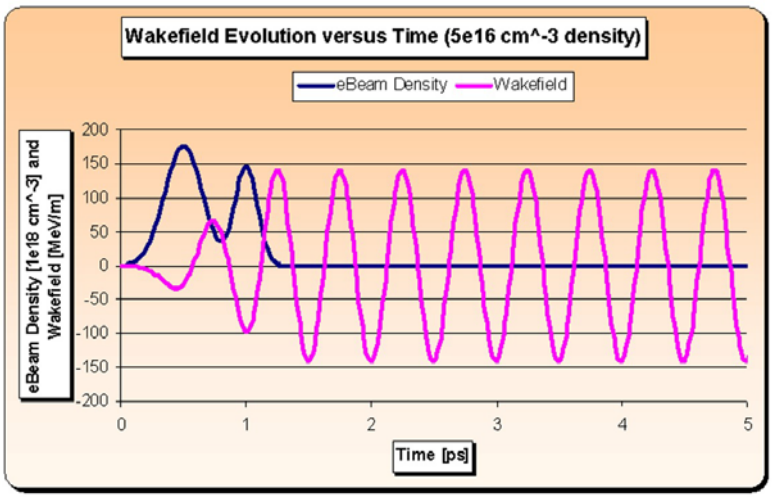

Fig. 2-32. 1-D PIC code simulation of double-bunches traveling through a plasma. (Courtesy of E. Kallos)

As with any wave phenomenon, the wakefields produced by the bunches can add constructively or destructively together. This effect can be seen more clearly in Fig. 2-33, which plots the model predictions for the energy loss or gain of the low-energy bunch. (Gain is represented by negative energy loss in Fig. 2-33.) The data are the red dots; the model predictions is the solid blue curve. For this particular set of data, gain was observed when the plasma was approximately 10^{16} cm^{-3}. The model predicts gain should also occur for the low-energy bunch at this density. Hence, we see very good agreement between the data and model.

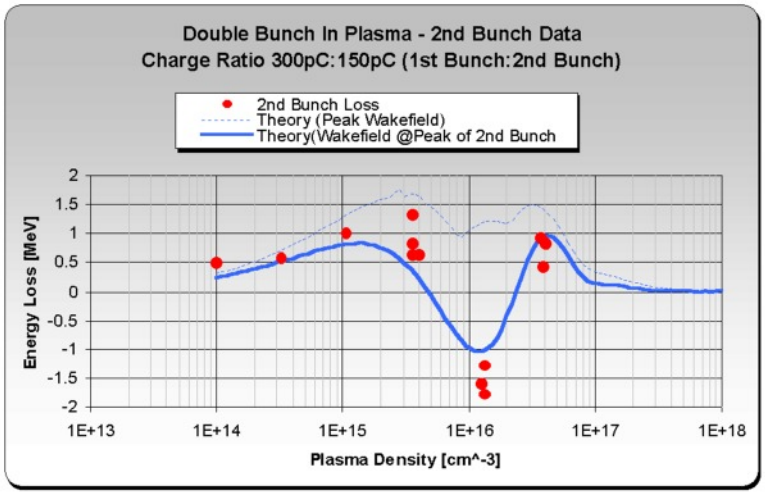

Fig. 2-33. 1-D PIC model prediction for energy gain and loss of the low-energy bunch versus plasma density. (Courtesy E. Kallos)

The dotted blue curve in Fig. 2-33 represents the combined peak of the wakefields from the two bunches. The depth of the dip in this curve is sensitive to the relative amount of charge in each bunch. This can seen be in Fig. 2-34. The red and green curves are for the case when the high-energy seed has twice the charge of the low-energy seed. The blue and brown curves are for the case when the charge ratio is reversed, i.e., high-energy seed has half the charge of the low-energy seed. We see a marked difference in the amount of energy gain or loss at 10^{16} cm^{-3} density. This implies the amount of gain or loss seen by the low-energy bunch is sensitive to the relative charge ratio between the two bunches. This may explain why energy loss is only seen in Fig. 2-31 at 10^{16} cm^{-3}, whereas, energy gain in observed in Fig. 2-32. The charge ratio was indeed different for the two sets of data.

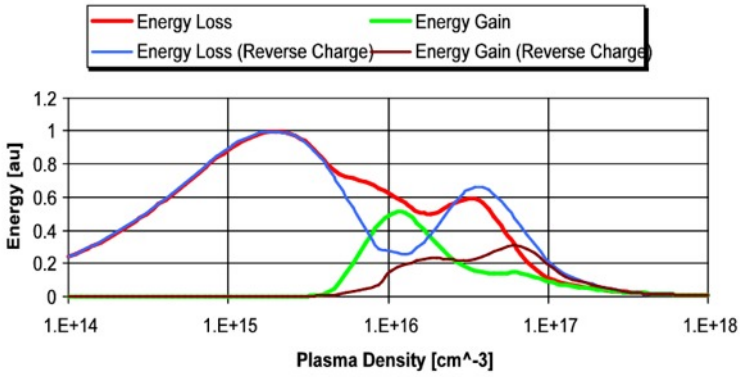

Fig. 2-34. 1-D PIC code predictions for energy gain or loss at two different charge ratios. (Courtesy of E. Kallos)

Prior to testing the chicane and the discovery of the double-bunch formation phenomenon, the ATF had already demonstrated the ability to generate two electron bunches from the linac by sending two laser pulses to the photoinjector. The second bunch was to serve as the witness bunch for probing the amplified wakefield. Adjusting the time delay between the laser pulses permitted varying the time delay between these two bunches. The nominal delay time is 20 ps. Because of this time delay, the two bunches intersect the RF field at different phases and, therefore, gain different amounts of energy. This results in approximately 2-3 MeV energy difference when they leave the linac.

Data was taken with the witness bunch following the double-bunch seed in the polypropylene capillary. Because the three bunches have three different mean energies and their energy profiles partially overlap, the resulting energy spectrum is complex. Figure 2-35(a) shows the spectrum of the three bunches when no plasma is present. The three bunches have been identified in the figure. The witness and low-energy seed bunch spectrums are saturated in order for the spectrometer camera to have enough sensitivity to detect the weaker high-energy seed signal.

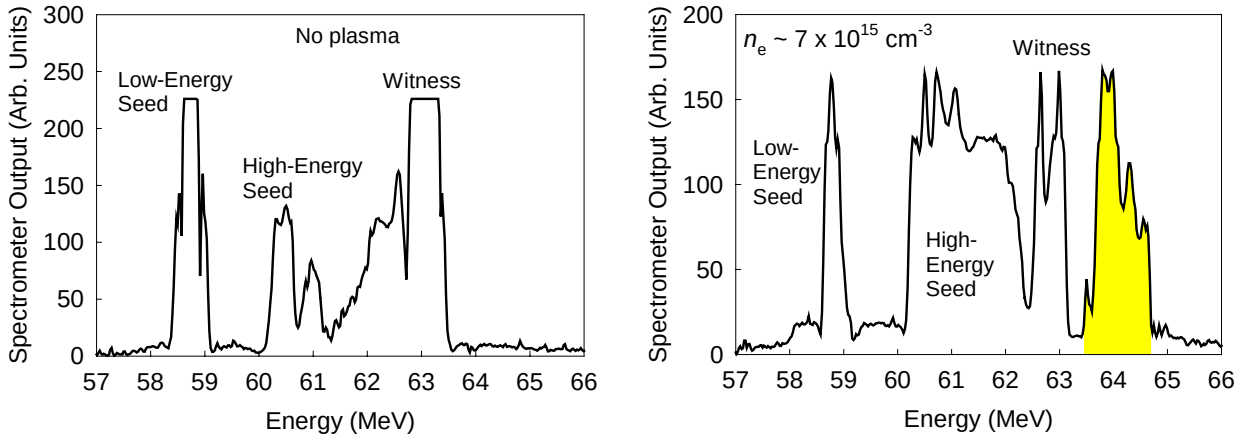

Fig. 2-35. Energy spectrums of double-bunch seeds with witness bunch. (a) With no plasma discharge. (b) With a plasma density of ~7 × 10^{15} cm^{-3}.

At a plasma density of roughly 7 × 10^{15} cm^{-3}, [Fig. 2-35(b)] there appears electrons (shaded yellow in the figure) with energies over 1 MeV higher than the witness. Assuming these electrons came from the witness, this would represent an energy gradient of >200 MeV/m.

Despite the apparent ability to accelerate witness bunch electrons, the highly complex and poorly understood energy spectrum of the three bunches, the wakefield sensitivity to the ratio of charge in the double bunches, and the inability to obtain the same bunch characteristics during different runs made using the three-bunch arrangement unsuitable for performing the seeded SM-LWFA experiment. Furthermore, subsequent tests where the high-energy slit was used to block one of the compressed bunches demonstrated that using only one of the bunches also produced unreliable wakefield formation. This is probably because the double-bunch formation process is a highly nonlinear one where slight changes in the beam tune can dramatically alter the compressed bunch characteristics, in particular the bunch length. If the bunch length changes, then the resonant plasma density also changes. Finding the correct plasma density becomes exceedingly difficult if the bunch length changes in an uncontrolled manner.

2.4.3 Seeded SM-LWFA Experiment Using Fast-rising Seed Bunch

During the latter half of the last year of the STELLA-LW program, the ATF developed a technique to compress the leading edge of the 1-ps bunch emitted from the photocathode without using the chicane. Tests as part of the multibunch PWFA experiment confirmed that this fast-rising bunch has a risetime of ~50 fs and it is capable of generating wakefields. However, the electron beam optics necessary to achieve this were only available on Beamline #2. Since the

double-bunch beam on Beamline #1 was not suitable for the seeded SM-LWFA experiment, the decision was made to move the experiment from Beamline #1 to Beamline #2.

This move required installing the 4-mm gas-filled capillary in a vacuum chamber on Beamline #2 and mounting new optics to deliver the TW CO_2 laser beam to Beamline #2. In addition, the CTS diagnostic had to be diassembled and reassembled on Beamline #2. This move occurred during November 2007 and the STELLA-LW program was slated to end on December 31, 2007. This meant there was only time for one run in December to perform the seeded SM-LWFA experiment on Beamline #2. There was also insufficient time to generate a witness bunch, which would have required delivering two laser pulses to the photocathode.

During the 2-week run in December, the first week was spent completing the setup and preliminary testing of the equipment in its new location. In particular, obtaining proper triggering of the Pyrocam-III camera was hampered by electrical noise and difficulties in finding the correct delay times. Data was taken during the second week of the run.

The new setup on Beamline #2 also included a means for monitoring the amount of laser light transmitted through the capillary. Earlier off-line tests with the laser focused in the capillary indicated that good transmission should occur when the discharge is present. However, during the alignment of the laser beam through the capillary on Beamline #2, just the opposite situation was found. Best transmission occurred with no gas or discharge in the capillary; worse transmission occurred with gas and the discharge on. To ensure a pre-pulse from the laser system was not creating a plasma that was blocking the main laser pulse, a saturable absorber was inserted at the output of the TW CO_2 laser. However, this did not help improve the transmission of the laser beam.

The amount of laser beam transmission varied from shot to shot from less than 20% to as high as 50%. Occasionally, there appeared to be no transmission. The fact the amount of transmission varied erratically made us suspect more than one effect may have been affecting the laser beam. The possible effects are:

1) Defocusing of the laser beam caused by laser-induced ionization of the plasma in the center of the capillary, thereby creating a negative lens effect. The defocused light would strike the inside walls of the capillary and not be transmitted.

2) Ablation of the capillary walls by the defocused laser beam, which could increase the local plasma density. The 4-mm, 1-mm diameter capillary was designed to fit within the Rayleigh range of the focused laser beam. Indeed, alignment tests with no gas or discharge indicate that the laser beam was being transmitted well through the capillary. The ablated material from the wall could increase the local plasma density enough to begin absorbing the laser beam, thereby further decreasing the amount of laser beam transmission.

Since the degree of laser-induced ionization and wall ablation would not necessarily be the same from shot to shot due to natural fluctuations in the laser output energy and the discharge characteristics, it is not surprising the amount of laser transmission varied greatly.

Although the poor laser transmission was an ominous sign that the experiment would not work, we attempted to perform the experiment nonetheless. With the fast-rising bunch sent through the 4-mm gas-filled capillary, the gas pressure and timing was adjusted until wakefield formation was confirmed by observing energy loss of the electrons on the Beamline #2 spectrometer. The laser beam was fired into the capillary with the *e*-beam present and the output from the Pyrocam-III camera was recorded. Despite varying the arrival time of the laser pulse

with respect to the *e*-beam over a wide range before and after the *e*-beam, no conclusive evidence of any Stokes signal was observed on the camera image.

A more sensitive photovoltaic detector (Noise Equivalent Power = 40 μW) was also tried instead of the Pyrocam-III camera. Once again no Stokes signal was observed.

2.5 DISCUSSION

As mentioned, earlier off-line tests of the TW CO_2 laser beam focused through the 4-mm capillary did not suffer from transmission problems. It is not certain why the transmission was adversely affected on Beamline #2. Although the laser beam transport system and focusing optics layout were similar between the off-line and Beamline #2 tests, they were not identical. In particular, the laser beam had to travel much further for the Beamline #2 tests. The beam shape can change during its propagation over the longer distance resulting in a different-shaped beam being focused into the capillary. This change may have been enough to alter the beam's affect on the plasma. Or, stated another way, for our particular configuration, the focusing of the TW CO_2 laser beam into the capillary may have been at a borderline condition where a small change could cause the laser beam to affect the plasma or not. Possibly during the off-line tests we happened to be on the side of the borderline where no effect occurred; on Beamline #2 we happened to be on the other side.

Subsequent to the run, it was discovered that the ATF laser was producing multiple laser pulses. It is highly likely multiple pulses were being delivered during the STELLA-LW run. If so, then it is certainly possible that the leading pulse might be the one responsible for initiating laser-induced ionization and/or wall ablation. This would interfere with transmission of the following pulses. Moreover, the total pulse energy as measured by the energy power meter was actually distributed among the multiple pulses. This means the peak power of any of the individual pulses was a factor of 3 to 4 times smaller than if all the energy had been within a single pulse. The lower peak power, which would be substantially less than 1 TW in each pulse, would be enough to prevent any Stokes signal.

Therefore, the absence of a Stokes signal could be due to several effects. First, if the laser beam was defocused by the plasma, then laser light would be lost and not reach the detector. Second, defocusing would also reduce the laser intensity, thereby preventing the self-modulation process from occurring. Third, the multiple laser pulses meant each pulse would have insufficient peak power to drive the SM-LWFA process. Fourth, if the laser beam was changing the on-axis plasma density, then it is probable the wakefield produced by the bunch would not survive. This is because the wakefield would no longer be resonant with the plasma density. Hence, there would be no Stokes signal because there is no wakefield.

The fact the laser beam appeared to be changing the plasma characteristics implies that the experiment performed on Beamline #2 was not under the conditions assumed during the modeling analysis. The modeling assumed a static plasma density and a well-behaved laser beam intensity distribution inside the plasma. It also obviously assumed a single laser pulse. Therefore, the failure to detect any Stokes radiation is not an indication that the seeded SM-LWFA theory and modeling is invalid; rather, the experiment as performed was not a legitimate test of the theory.

Besides ensuring delivery of a single laser pulse, a valid test of the theory would require eliminating the laser beam affecting the plasma. Probably the best way to do this is to guide the

laser beam through the capillary to avoid defocusing and ablation effects. However, the capillary could not guide the laser beam and at the same time achieve the needed laser intensity to drive the self-modulation process. This is because a plasma density of 3×10^{17} cm^{-3}, which is the resonant density for the fast-rising seed bunch, yields a parabolic density profile inside the capillary corresponding to a matched laser waist size for guiding that is too large, i.e., for the available laser peak power, the matched waist size would result in a laser intensity that is too low. The only way to overcome this is to increase the laser peak power, which was not available, or operate at a higher plasma density requiring a faster rising bunch, which was also not available. Therefore, in hindsight it is not clear the ATF had the capabilities required to test the seeded SM-LWFA process.

2.6 NEED FOR ADVANCED CAPILLARY DISCHARGE DESIGN

One can argue that the inability of the ATF to provide higher laser peak power or faster-rising bunches is not a shortcoming of the facility, but rather it represents the current state-of-the-art in these technologies. Although there are ways to push this state-of-the-art, it would be costly and time-consuming to achieve this. On the other hand, if there were ways to improve the capabilities of the plasma source, i.e., the capillary discharge, then this might be a less costly and easier way to achieve conditions necessary to test schemes such as seeded SM-LWFA. This is part of the motivation for the discussion given in this subsection where we briefly present ideas for improving the capabilities of capillary discharges. These formed the basis for a proposal that was submitted to the U.S. Department of Energy (DOE) to demonstrate these new ideas.

Capillary discharge plasmas have proven to be an effective plasma medium for LWFA. They have demonstrated essential properties required for the LWFA plasma target: consistent shot-to-shot plasma densities and a quasi-parabolic density profile that provides laser guiding along the plasma column. Looking beyond these early achievements, we see that the next step for realizing practical plasma-based accelerators will require addressing certain critical issues related to capillary discharges. These issues include (1) the seemingly contradictory requirements of low plasma density (to enable long wakefield dephasing lengths and usage of longer laser/*e*-beam pulse lengths) and adequate laser guiding; (2) for the case of gas-filled capillaries, the violation of the exquisite vacuum necessary in the beamline by the quantities of gas injected into the beamline by the capillary; (3) high pulse repetition frequency (PRF) in order to achieve useful average beam currents; and (4) ease of scalability to long plasma section lengths needed to achieve high net energy gain. While plasma-discharge capillaries may appear to be a niche technology with a limited user base, it is actually a "hinge" technology that is a vital component in plasma-based accelerator development. For example, besides LWFA, capillary discharges can be used in other plasma-based applications, such as plasma wakefield acceleration (PWFA), plasma beatwave acceleration (PBWA), hybrid LWFA/PWFA schemes, plasma lenses, XUV lasers, higher-harmonic-generation (HHG), and particle acceleration by stimulated emission of radiation (PASER) [2-30]. All these applications would benefit with the availability of improved capillary discharge designs.

The primary goal of our proposed program to the DOE is to demonstrate advanced concepts for capillary discharge designs that address the preceding issues. Two novel concepts were proposed. The first is called standing-wave excitation whereby a dynamically changing plasma density profile is created inside the capillary by either modulating the discharge current or, alternately, by having the capillary surrounded by a solenoid magnet whose *B*-field oscillates. By applying this oscillating field, radial pressure waves are launched from the capillary walls

and propagate inwards. This sets up a standing-wave density pattern with a J_0 Bessel structure. With appropriate selection of the oscillating frequency, the central lobe of the J_0 pattern can have a deeper parabolic-like profile, even at low plasma densities, than the one created in a conventional capillary that relies on only thermal gradients to establish the parabolic profile. This approach can help solve the problem of guiding tightly-focused laser beams at low plasma densities.

The second concept is to utilize a transverse-flow discharge geometry with the gas flowing orthogonal to the laser beam and *e*-beam axis. This arrangement employs ducts connected to the sides of the capillary to inject gas and remove it from the capillary. This distributed injection and removal system reduces the amount of gas escaping out the ends of the capillary and into the beamline vacuum, thereby relaxing demands on the pumping system. The electrodes can also be oriented along the sides of the capillary so that the discharge is transverse to the laser beam. This geometry is essentially similar to one used in transverse-excited gas discharge lasers. Key features of our transverse-flow discharge scheme are that it still enables the creation of a parabolic density profile for guiding the laser beam and it is compatible with incorporating the standing-wave excitation concept. It is also well suited for (a) operation at high PRF; (b) scaling to longer discharge lengths, (c) plasma density tapering, i.e., varying the plasma density along the *e*-beam direction, and (d) the ability to have elliptically-shaped plasma cross-sections, thereby permitting acceleration of "ribbon" *e*-beams to combat space-charge spreading.

At the time of the writing of this final report, our proposal for the advanced capillary discharge development was still under review by DOE.

2.7 CONCLUSION

Due to technology limitations, it was not possible to perform conclusive tests of the pseudo-resonant LWFA and seeded self-modulated LWFA schemes. If higher laser peak power were available in a single laser pulse, then both experiments could have been performed. Achieving higher peak power of the ATF CO_2 laser system is possible, but it involves costly and time-consuming upgrades, and it was not practical to achieve within the period of performance of the STELLA-LW program.

Although the STELLA-LW program did not reach its goal, our collaboration with the USC on their multibunch PWFA experiment did provide helpful contributions to their experiment and vice versa. This collaboration also resulted in the development of other new ideas related to creating multibunches [2-31].

REFERENCES

2-1) See for example, W. P. Leemans in *Advanced Accelerator Concepts*, Jun. 21-26, 2004, Stony Brook, NY, AIP Conference Proceedings No. 737, V. Yakimenko, Ed., (American Institute of Physics, New York, 2004), p. 11-28.

2-2) T. Tajima and J. M. Dawson, Phys. Rev. Lett. **43**, 267 (1979); L. M. Gorbunov, and V. I. Kirsanov, *Sov. Phys. JETP* **66**, 290 (1987).

2-3) N. E. Andreev, L. M. Gorbunov, V .I. Kirsanov, A. A. Pogosova, and R. R. Ramazashvili, Pis'ma Zh. Eksp. Teor. Fiz. **55**, 551 (1992) [JETP Lett. **55**, 571-576 (1992)].

2-4) P. Chen, J. M. Dawson, R. W. Huff, and T. Katsouleas, Phys. Rev. Lett. **54**, 693 (1985).

2-5) R. B. Palmer, J. Appl. Phys. **43**, 3014 (1972).

2-6) W. D. Kimura, *et al*., Phys. Rev. Lett. **92**, 054801 (2004).

2-7) W. D. Kimura, *et al*., Phys. Rev. ST Accel. Beams **7**, 091301 (2004).

2-8) N. E. Andreev, *et al*., Phys. Rev. ST Accel. Beams **9**, 031303 (2006).

2-9) N. E. Andreev, *et al*., Phys. Rev. ST Accel. Beams **6**, 041301 (2003).

2-10) W. D. Kimura, *et al*., IEEE Trans. Plasma Sci. **33**, 3-7 (2005).

2-11) L. C. Steinhauer, W. D. Kimura, and R. N. Agarwal, in Proceedings of International Conference on Lasers 2001, Tucson, AZ, Dec. 3-7, 2001, V. J. Corcoran and T. A. Corcoran, Editors, (STS Press, McLean, 2002), pp. 159-163.

2-12) N.E. Andreev, L.M. Gorbunov, V.I. Kirsanov, Fizika Plasmy, 21, 872 (1995) [Plasma Physics Reports 21, 824 (1995)]; Phys. Plasmas **2**, 2573 (1995).

2-13) M. Fomyts'kyi, C. Chiu, M. Downer, and F. Grigsby, Phys. Plasmas **12**, 023103 (2005).

2-14) W. D. Kimura, et al., Phys. Rev. ST Accel. Beams **4**, 101301 (2001).

2-15) N. E. Andreev, *et al*., Phys. Plasmas **13**, 053109 (2006).

2-16) I. V. Pogorelsky, Nucl. Instrum. and Methods in Phys. Res. A **410**, 524-531 (1998).

2-17) N. E. Andreev, S. V. Kuznetsov, and I. V. Pogorelsky**,** Phys. Rev. ST – Accel. Beams **3**, 021301 (2000).

2-18) S. V. Bulanov, *et al*., IEEE Trans. Plasma Sci. **24**, 393-399 (1996).

2-19) Z. Najmudin, *et al*., Physics Plasmas **10**, 2071-2077 (2003).

2-20) A. Butler, D. J. Spencer, and S. M. Hooker, Phys. Rev. Lett. **89**, 185003 (2002).

2-21) E. Kallos, *et al*., in Proceedings of 2005 IEEE Particle Accelerator Conference Proceedings, IEEE Cat. No. 05CH37623C, 3384-3386 (2005).

2-22) *Principles of Laser Plasmas*, edited by G. Bekefi, (John Wiley and Sons, 1976), Chap. 13.

2-23) D. Stolyarov, *et al*., in *Advanced Accelerator Concepts*, Jul. 10-15, 2006, Lake Geneva, WI, AIP Conference Proceedings No. 877, M. Conde and C. Eyberger, Eds., (American Institute of Physics, New York, 2006), p. 784-791.

2-24) BLIS manufactured by RadiaBeam Technologies.

2-25) A. Murokh, *et al*., Nucl. Inst. Meth. Phys. Res., A **410**, 452 (1998).

2-26) C. E. Clayton, *et al*., Phys. Rev. Lett. **54**, 2343 (1985).

2-27) A Ting, *et al*., Phys. Rev. Lett. **77**, 5377 (1996).

2-28) N. Andreev, *et al*., Phys. Plasmas. **13**, 053109 (2006).

2-29) R. Agustsson, UCLA, M.S. thesis, 2004.

2-30) S. Banna, V. Berezosky, and L. Schächter, Phys. Rev. Lett. **97**, 134801 (2006).

2-31) V. E. Yakimenko, *et al*., in Proceedings of FEL 2006, BESSY, Berlin, Germany, p. 481.

SECTION 3
PAPERS AND PRESENTATIONS

3.1 PAPERS

The following papers were published from 2003-2007 during the STELLA-LW program.

1. N. E. Andreev, S. V. Kuznetsov, A. A. Pogosova, L. C. Steinhauer, and W. D. Kimura, "Modeling of Laser Wakefield Acceleration at CO_2 Laser Wavelengths," Phys. Rev. ST Accel. Beams **6**, 041301 (2003).
2. F. Zhou, D. B. Cline, and W. D. Kimura, "Beam Dynamics Analysis of Femtosecond Microbunches Produced by the Staged Electron Laser Acceleration Experiment," Phys. Rev. ST Accel. Beams **6**, 054201 (2003).
3. L. C. Steinhauer and W. D. Kimura, "Slow Waves in Microchannel Metal Waveguides and Application to Particle Acceleration," Phys. Rev. ST Accel. Beams **6**, 061302 (2003).
4. W. D. Kimura, M. Babzien, I. Ben-Zvi, L. P. Campbell, D. B. Cline, C. E. Dilley, J. C. Gallardo, S. C. Gottschalk, K. P. Kusche, R. H. Pantell, I. V. Pogoresky, D. C. Quimby, J. Skaritka, L. C. Steinhauer, V. Yakimenko, and F. Zhou, "Demonstration of High-Trapping Efficiency and Narrow Energy Spread in a Laser-Driven Accelerator," Phys. Rev. Lett. **92**, 054801 (2004).
5. W. D. Kimura, L. P. Campbell, C. E. Dilley, S. C. Gottschalk, D. C. Quimby, M. Babzien, I. Ben-Zvi, J. C. Gallardo, K. P. Kusche, I. V. Pogorelsky, J. Skaritka, V. Yakimenko, D. B. Cline, F. Zhou, L. C. Steinhauer, and R. H. Pantell, "Detailed Experimental Results for High-Trapping Efficiency and Narrow Energy Spread in a Laser-Driven Accelerator," Phys. Rev. ST Accel. Beams **7**, 091301 (2004).
6. I. V. Pogorelsky, "Experiments on Energy Exchange in Laser/*E*-Beam Interactions," Proceedings of SPIE 5482, 62 (2004); presented at Laser Optics, St. Petersburg, Russia, 2004.
7. W. D. Kimura and S. M. Lidia, "EM Structure-Based Accelerators Working Group Summary," in *Advanced Accelerator Concepts*, Jun. 21-26, 2004, Stony Brook, NY, AIP Conference Proceedings No. 737, V. Yakimenko, Ed., (American Institute of Physics, New York, 2004), p. 193-205.
8. W. D. Kimura, P. Musumeci, D. C. Quimby, S. C. Gottschalk, and C. Pellegrini, "Conceptual Design for a 1-GeV IFEL Accelerator," in *Advanced Accelerator Concepts*, Jun. 21-26, 2004, Stony Brook, NY, AIP Conference Proceedings No. 737, V. Yakimenko, Ed., (American Institute of Physics, New York, 2004), p. 251-257.
9. W. D. Kimura, M. Babzien, I. Ben-Zvi, L. C. Campbell, D. B. Cline, C. E. Dilley, J. C. Gallardo, S. C. Gottschalk, K. P. Kusche, R. H. Pantell, I. V. Pogorelsky, D. C. Quimby, J. Skaritka, L. C. Steinhauer, V. Yakimenko, and F. Zhou, "Model Comparisons with STELLA Experimental Results," in *Advanced Accelerator Concepts*, Jun. 21-26, 2004, Stony Brook, NY, AIP Conference Proceedings No. 737, V. Yakimenko, Ed., (American Institute of Physics, New York, 2004), p. 335-341.

10. I.V. Pogorelsky, I.V. Pavlishin, I. Ben-Zvi, V. Yakimenko, T. Kumita, Y. Kamiya, A. Zigler, A. Diublov, N. Andreev, N. Bobrova, and P. Sasorov, "Experiments on Laser and *E*-Beam Transport and Interaction in a Plasma Channel," in *Advanced Accelerator Concepts*, Jun. 21-26, 2004, Stony Brook, NY, AIP Conference Proceedings No. 737, V. Yakimenko, Ed., (American Institute of Physics, New York, 2004), p. 504-511.

11. W. D. Kimura, N. E. Andreev, M. Babzien, I. Ben-Zvi, D. B. Cline, C. E. Dilley, S. C. Gottschalk, S. M. Hooker, K. P. Kusche, S. V. Kuznetsov, R. H. Pantell, I. V. Pavlishin, I. V. Pogorelsky, A. A. Pogosova, L. C. Steinhauer, A. Ting, V. Yakimenko, A. Zigler, and F. Zhou, "Laser Wakefield Acceleration Driven by ATF CO_2 Laser (STELLA-LW)," in *Advanced Accelerator Concepts*, Jun. 21-26, 2004, Stony Brook, NY, AIP Conference Proceedings No. 737, V. Yakimenko, Ed., (American Institute of Physics, New York, 2004), p. 534-540.

12. L. C. Steinhauer and W. D. Kimura, "Analytical Modeling of Pseudo-Resonant LWFA in a Capillary Discharge," in *Advanced Accelerator Concepts*, Jun. 21-26, 2004, Stony Brook, NY, AIP Conference Proceedings No. 737, V. Yakimenko, Ed., (American Institute of Physics, New York, 2004), p. 865-870.

13. W. D. Kimura, N. E. Andreev, M. Babzien, I. Ben-Zvi, D. B. Cline, C. E. Dilley, S. C. Gottschalk, S. M. Hooker, K. P. Kusche, S. V. Kuznetsov, R. H. Pantell, I. V. Pavlishin, I. V. Pogorelsky, A. A. Pogosova, L. C. Steinhauer, A. Ting, V. Yakimenko, A. Zigler, and F. Zhou, "Pseudo-Resonant Laser Wakefield Acceleration Driven by 10.6 μm Laser Light," IEEE Trans. Plasma Sci. **33**, 3-7 (2005).

14. W. D. Kimura, "Microbunching," in *Femtosecond Beam Science*, M. Uesaka, Ed., (Imperial College Press, London, 2005), p. 63-71.

15. F. Zhou, D. Cline, M. Babzien, V. Yakimenko, and W. D. Kimura, "Manipulations of Double Beams in One RF Period for STELLA SM-LWFA Experiment", in Proceedings of 2005 IEEE Particle Accelerator Conference Proceedings, IEEE Cat. No. 05CH37623C, 2312-2314 (2005).

16. E. Kallos, T. Katsouleas, P. Muggli, I. Ben-Zvi, I. Pogorelsky, V. Yakimenko, I. Pavlishin, K. Kusche, M. Babzien, F. Zhou, and W. D. Kimura, "A Multibunch Plasma Wakefield Accelerator", in Proceedings of 2005 IEEE Particle Accelerator Conference Proceedings, IEEE Cat. No. 05CH37623C, 3384-3386 (2005).

17. I. V. Pogorelsky, M. Babzien, K. P. Kusche, I. V. Pavlishin, V. Yakimenko, C. E. Dilley, S. C. Gottschalk, W. D. Kimura, T. Katsouleas, P. Muggli, E. Kallos, L. C. Steinhauer, A. Zigler, N. Andreev, D. B. Cline, F. Zhou, "Plasma-based Advanced Accelerators at the Brookhaven Accelerator Test Facility," Laser Physics **16**, 259 (2006).

18. W. D. Kimura, N. E. Andreev, M. Babzien, I. Ben-Zvi, D. B. Cline, C. E. Dilley, S. C. Gottschalk, S. M. Hooker, K. P. Kusche, S. V. Kuznetsov, I. V. Pavlishin, I. V. Pogorelsky, A. A. Pogosova, L. C. Steinhauer, A. Ting, V. Yakimenko, A. Zigler, and F. Zhou, "Inverse Free Electron Lasers and Laser Wakefield Acceleration Driven by CO_2 Lasers," Phil. Trans. R. Soc. A **364**, 611-622 (2006).

19. I. V. Pogorelsky, M. Babzien, K. P. Kusche, I. V. Pavlishin, V. Yakimenko, C. E. Dilley, S. C. Gottschalk, W. D. Kimura, T. Katsouleas, P. Muggli, E. Kallos, L. C. Steinhauer, A. Zigler, N. Andreev, D. B. Cline, and F. Zhou, "Plasma-Based Advanced Accelerators at the Brookhaven Accelerator Test Facility," Laser Physics, **16**, 259–266 (2006).

20. N. E. Andreev, S. V. Kuznetsov, A. A. Pogosova, L. C. Steinhauer, and W. D. Kimura, "Seeded Self-Modulated Laser Wakefield Acceleration," Phys. Rev. ST Accel. Beams **9**, 031303 (2006).

21. L. C. Steinhauer, and W. D. Kimura, "Quasi-Static Capillary Discharge Plasma Model," Phys. Rev. ST Accel. Beams **9**, 081301 (2006).

22. E. Kallos, P. Muggli, T. Katsouleas, V. Yakimenko, D. Stolyarov, I. Pogorelsky, I. Pavlishin, K. Kusche, M. Babzien, I. Ben-Zvi, and W. D. Kimura, "Resonant Plasma Wakefield Experiment: Plasma Simulations and Multibunched Electron Beam Diagnostics," in *Advanced Accelerator Concepts*, Jul. 10-15, 2006, Lake Geneva, WI, AIP Conference Proceedings No. 877, M. Conde and C. Eyberger, Eds., (American Institute of Physics, New York, 2006), p. 520-526.

23. W. D. Kimura, V. Yakimenko, M. Babzien, X. Ding, E. Kallos, K. P. Kusche, I. V. Pavlishin, I. V. Pogorelsky, D. Stolyarov, and F. Zhou, "Subpicosecond Double Electron Bunch Generation," in *Advanced Accelerator Concepts*, Jul. 10-15, 2006, Lake Geneva, WI, AIP Conference Proceedings No. 877, M. Conde and C. Eyberger, Eds., (American Institute of Physics, New York, 2006), p. 527-533.

24. W. D. Kimura, N. E. Andreev, M. Babzien, D. B. Cline, X. Ding, S. M. Hooker, E. Kallos, T. C. Katsouleas, K. P. Kusche, S. V. Kuznetsov, P. Muggli, I. V. Pavlishin, I. V. Pogorelsky, A. A. Pogosova, L. C. Steinhauer, D. Stolyarov, A. Ting, V. Yakimenko, A. Zigler, and F. Zhou, "Update on Seeded SM-LWFA and Pseudo-Resonant LWFA Experiments – (STELLA-LW)," in *Advanced Accelerator Concepts*, Jul. 10-15, 2006, Lake Geneva, WI, AIP Conference Proceedings No. 877, M. Conde and C. Eyberger, Eds., (American Institute of Physics, New York, 2006), p. 534-540.

25. N. E. Andreev, S. V. Kuznetsov, A. A. Pogosova, L. C. Steinhauer, and W. D. Kimura, "Expanded Model Prediction for Seeded SM-LWFA and Pseudo-Resonant LWFA," in *Advanced Accelerator Concepts*, Jul. 10-15, 2006, Lake Geneva, WI, AIP Conference Proceedings No. 877, M. Conde and C. Eyberger, Eds., (American Institute of Physics, New York, 2006), p. 714-720.

26. L. C. Steinhauer and W. D. Kimura, "Gas-Filled Capillary Model," in *Advanced Accelerator Concepts*, Jul. 10-15, 2006, Lake Geneva, WI, AIP Conference Proceedings No. 877, M. Conde and C. Eyberger, Eds., (American Institute of Physics, New York, 2006), p. 777-783.

27. D. Stolyarov, I. Pavlishin, K. Kusche. M. Babzien, W. Kimura, P. Muggli, E. Kallos, and V. Yakimenko, "Plasma Density Measurements in Hydrogen-Filled and Plastic Ablation Discharge Capillaries Based on Stark Broadening of Atomic Hydrogen Spectral Lines," in *Advanced Accelerator Concepts*, Jul. 10-15, 2006, Lake Geneva, WI, AIP Conference Proceedings No. 877, M. Conde and C. Eyberger, Eds., (American Institute of Physics, New York, 2006), p. 784-791.

28. C. Sung, S. Ya. Tochitsky, S. Reiche, S. C. Gottschalk, W.D. Kimura, J. B. Rosenzweig, C. Pellegrini, C. Joshi, "Development of a Waveguide FEL Seeded in the 1-3 THz Range for Microbunching Experiment at the Neptune Laboratory," in *Advanced Accelerator Concepts*, Jul. 10-15, 2006, Lake Geneva, WI, AIP Conference Proceedings No. 877, M. Conde and C. Eyberger, Eds., (American Institute of Physics, New York, 2006), p. 895-902.

29. V. E. Yakimenko, M. Babzien, K. P. Kusche, X. Ding, E. Kallos, P. Muggli W. D. Kimura, F. Zhou, "Generation and Characterization of the Microbunched Beams in the Range from 0.3 To 500 Femtoseconds," in Proceedings of FEL 2006, BESSY, Berlin, Germany, 481-484 (2006).

30. E. Kallos, T. Katsouleas, P. Muggli, I. Pavlishin, I. Pogorelsky, D. Stolyarov, V. Yakimenko, W. D. Kimura, "Plasma Wakefield Acceleration Utilizing Multiple Electron Bunches", in Proceedings of 2007 IEEE Particle Accelerator Conference Proceedings, 3070-3072 (2007).

31. P. Muggli, E. Kallos, V. E. Yakimenko, M. Babzien, and K. P. Kusche, and W. D. Kimura, "Generation And Characterization of Microbunched Beams with a Wire Mesh Mask", in Proceedings of 2007 IEEE Particle Accelerator Conference Proceedings, 3079-3081 (2007).

32. P. Muggli, W. D. Kimura, E. Kallos, T. C. Katsouleas, K. P. Kusche, I. V. Pavlishin, D. Stolyarov, and V. E. Yakimenko, "Plasma Wakefield Acceleration Experiments Using Two Subpicosecond Electron Bunches", in Proceedings of 2007 IEEE Particle Accelerator Conference Proceedings, 3073-3074 (2007).

33. X. Ding, D. B. Cline, M. Babzien, K. Kusche, V. Yakimenko, F. Zhou, W. D. Kimura, "Generation and Analysis of Subpicosecond Double Electron Bunch at the Brookhaven Accelerator Test Facility", in Proceedings of 2007 IEEE Particle Accelerator Conference Proceedings, 4132-4134 (2007).

3.2 PRESENTATIONS

The following talks were presented from 2003-2007 during the STELLA-LW program.

1. W. D. Kimura, M. Babzien, I. Ben-Zvi, L. C. Campbell, D. B. Cline, C. E. Dilley, J. C. Gallardo, S. C. Gottschalk, K. P. Kusche, R. H. Pantell, I. V. Pogoresky, D. C. Quimby, J. Skaritka, L. C. Steinhauer, V. Yakimenko, and F. Zhou, "Staged Laser Acceleration Using Upgraded ATF CO_2 Laser," 2003 Particle Accelerator Conference, Portland, OR, May 12-16, 2003, Paper TPPG048.

2. W. D. Kimura, P. Musumeci, D. C. Quimby, S. C. Gottschalk, and C. Pellegrini, "Conceptual Design for a 1-GeV IFEL Accelerator," 11th Workshop on Advanced Accelerator Concepts, Jun. 21-26, 2004, Stony Brook, NY.

3. L. C. Steinhauer and W. D. Kimura, "Analytical Modeling of Pseudo-Resonant LWFA in a Capillary Discharge," 11th Workshop on Advanced Accelerator Concepts, Jun. 21-26, 2004, Stony Brook, NY.

4. W. D. Kimura, N. E. Andreev, M. Babzien, I. Ben-Zvi, D. B. Cline, C. E. Dilley, S. C. Gottschalk, S. M. Hooker, K. P. Kusche, S. V. Kuznetsov, R. H. Pantell, I. V. Pavlishin, I. V. Pogorelsky, A. A. Pogosova, L. C. Steinhauer, A. Ting, V. Yakimenko, A. Zigler, and F. Zhou, "Laser Wakefield Acceleration Driven by ATF CO_2 Laser (STELLA-LW)" 11th Workshop on Advanced Accelerator Concepts, Jun. 21-26, 2004, Stony Brook, NY.

5. W. D. Kimura, M. Babzien, I. Ben-Zvi, L. C. Campbell, D. B. Cline, C. E. Dilley, J. C. Gallardo, S. C. Gottschalk, K. P. Kusche, R. H. Pantell, I. V. Pogorelsky, D. C. Quimby, J. Skaritka, L. C. Steinhauer, V. Yakimenko, and F. Zhou, "Model Comparisons with STELLA Experimental Results," 11th Workshop on Advanced Accelerator Concepts, Jun. 21-26, 2004, Stony Brook, NY.

6. W. D. Kimura, N. E. Andreev, M. Babzien, I. Ben-Zvi, D. B. Cline, C. E. Dilley, S. C. Gottschalk, S. M. Hooker, K. P. Kusche, S. V. Kuznetsov, R. H. Pantell, I. V. Pavlishin, I. V. Pogorelsky, A. A. Pogosova, L. C. Steinhauer, A. Ting, V. Yakimenko, A. Zigler, and F. Zhou, "Pseudo-Resonant Laser Wakefield Acceleration Driven by 10.6 μm Laser Light," 31st IEEE International Conference on Plasma Science, Jun. 28-Jul. 1, 2004, Baltimore, MD, Paper 2A9-10.

7. F. Zhou, D. Cline, M. Babzien, V. Yakimenko, and W. D. Kimura, "Manipulations of Double Beams in One RF Period for STELLA SM-LWFA Experiment", Particle Accelerator Conference 2005, May 16-20, 2005, Knoxville, TN, Paper TPAT034.

8. E. Kallos, T. Katsouleas, P. Muggli, M. Babzien, I. Ben-Zvi, K. Kusche, I. Pavlishin, I. Pogorelsky, V. Yakimenko, W. D. Kimura, and F. Zhou., "A Multibunch Plasma Wakefield Accelerator", Particle Accelerator Conference 2005, May 16-20, 2005, Knoxville, TN, Paper TPAE057.

9. W. D. Kimura, "Inverse Free Electron Lasers and Laser Wakefield Acceleration Driven by CO_2 Lasers," Royal Society Scientific Discussion Meeting on Laser-Driven Plasma Accelerators: New Sources of Energetic Particles and Radiation, Jun. 6-7, 2005, London, United Kingdom, invited talk.

10. I. V. Pogorelsky, M. Babzien, K. P. Kusche, I. V. Pavlishin, V. Yakimenko, C. E. Dilley, S. C. Gottschalk, W. D. Kimura, T. Katsouleas, P. Muggli, E. Kallos, L. C. Steinhauer, A. Zigler, N. Andreev, D. B. Cline, F. Zhou, "Plasma-based Advanced Accelerators at the Brookhaven Accelerator Test Facility," presented at 14th International Conference on Laser Science 2005 (Kyoto, Japan), July 4-8, 2005.

11. W. D. Kimura, N. E. Andreev, M. Babzien, I. Ben-Zvi, X. Ding, D. B. Cline, S. M. Hooker, K. P. Kusche, S. V. Kuznetsov, I. V. Pavlishin, I. V. Pogorelsky, A. A. Pogosova, L. C. Steinhauer, D. Stolyarov, A. Ting, V. Yakimenko, and A. Zigler, "Update on Seeded SM-LWFA and Pseudo-Resonant LWFA Experiments – (STELLA-LW)" 12th Workshop on Advanced Accelerator Concepts, Jul. 10-15, 2006, Lake Geneva, WI.

12. W. D. Kimura, N. E. Andreev, M. Babzien, I. Ben-Zvi, D. B. Cline, S. M. Hooker, K. P. Kusche, S. V. Kuznetsov, I. V. Pavlishin, I. V. Pogorelsky, A. A. Pogosova, L. C. Steinhauer, D. Stoylarov, A. Ting, V. Yakimenko, and A. Zigler, "Expanded Model Predictions for Seeded SM-LWFA and Pseudo-Resonant LWFA" 12th Workshop on Advanced Accelerator Concepts, Jul. 10-15, 2006, Lake Geneva, WI.

13. L. C. Steinhauer and W. D. Kimura, "Gas-Filled Capillary Model," 12th Workshop on Advanced Accelerator Concepts, Jul. 10-15, 2006, Lake Geneva, WI.

14. W. D. Kimura, M. Babzien, X. Ding, K. P. Kusche, I. V. Pavlishin, I. V. Pogorelsky, D. Stoylarov, V. Yakimenko, and F. Zhou, “Subpicosecond Double Electron Bunch Generation” 12th Workshop on Advanced Accelerator Concepts, Jul. 10-15, 2006, Lake Geneva, WI.

15. W. D. Kimura, M. Babzien, K. P. Kusche, I. V. Pavlishin, I. V. Pogorelsky, D. Stoylarov, V. Yakimenko, and F. Zhou, “Ultrafast Diagnostic Techniques Used In STELLA-LW Experiment” 12th Workshop on Advanced Accelerator Concepts, Jul. 10-15, 2006, Lake Geneva, WI.

16. D. Stolyarov, I. Pavlishin, K. Kusche. M. Babzien, W. Kimura, P. Muggli, E. Kallos, and V. Yakimenko, “Plasma Density Measurements in Hydrogen-Filled and Plastic Ablation Discharge Capillaries Based on Stark Broadening of Atomic Hydrogen Spectral Lines,” 12th Workshop on Advanced Accelerator Concepts, Jul. 10-15, 2006, Lake Geneva, WI.

17. E. Kallos, P. Muggli, T. Katsouleas, V. Yakimenko, D. Stolyarov, I. Pogorelsky, I. Pavlishin, K. Kusche, M. Babzien, I. Ben-Zvi, and W. D. Kimura, “Resonant Plasma Wakefield Experiment: Plasma Simulations and Multibunched Electron Beam Diagnostics,” 12th Workshop on Advanced Accelerator Concepts, Jul. 10-15, 2006, Lake Geneva, WI.

18. W. D. Kimura, “Plasma Wakefield Acceleration,” University of Washington, Seattle, WA, Nov. 13, 2006, invited lecture.

19. E. Kallos, T. Katsouleas, P. Muggli, I. Pavlishin, I. Pogorelsky, D. Stolyarov, V. Yakimenko, W. D. Kimura, “Plasma Wakefield Acceleration Utilizing Multiple Electron Bunches”, Particle Accelerator Conference 2007, Jun. 25-29, 2007, Albuquerque, NM, Paper THPMS031.

20. P. Muggli, E. Kallos, V. E. Yakimenko, M. Babzien, and K. P. Kusche, and W. D. Kimura, “Generation And Characterization of Microbunched Beams with a Wire Mesh Mask”, Particle Accelerator Conference 2007, Jun. 25-29, 2007, Albuquerque, NM, Paper THPMS034.

21. P. Muggli, W. D. Kimura, E. Kallos, T. C. Katsouleas, K. P. Kusche, I. V. Pavlishin, D. Stolyarov, and V. E. Yakimenko, “Plasma Wakefield Acceleration Experiments Using Two Subpicosecond Electron Bunches”, Particle Accelerator Conference 2007, Jun. 25-29, 2007, Albuquerque, NM, Paper THPMS032.

22. X. Ding, D. B. Cline, M. Babzien, K. Kusche, V. Yakimenko, F. Zhou, W. D. Kimura, “Generation and Analysis of Subpicosecond Double Electron Bunch at the Brookhaven Accelerator Test Facility”, Particle Accelerator Conference 2007, Jun. 25-29, 2007, Albuquerque, NM, Paper FRPMS059.

Seeded self-modulated laser wakefield acceleration

APPENDIX A

N. E. Andreev, S. V. Kuznetsov, and A. A. Pogosova
Institute for High Energy Densities, Russian Academy of Sciences, Izhorskaya 13/19, Moscow 125412, Russia

L. C. Steinhauer
University of Washington, Redmond Plasma Physics Laboratory, Redmond, Washington 98052 USA

W. D. Kimura*
STI Optronics, Inc., Bellevue, Washington 98004 USA
(Received 13 January 2006; published 31 March 2006)

A new approach to laser-wakefield acceleration (LWFA) has been analyzed. A seed electron beam bunch precedes the laser pulse into the plasma. This seed bunch initiates formation of plasma waves via a plasma wakefield acceleration mechanism. The amplitude of the plasma waves is subsequently amplified by the laser pulse via a self-modulated LWFA (SM-LWFA) process. This method enables the generation of strong wakefields even when the laser pulse by itself has characteristics that are insufficient for driving resonant LWFA or SM-LWFA. Another advantage is the wakefield formation begins at the seed bunch and does not start from noise as typically occurs in SM-LWFA. This feature may be helpful when the phase of the wakefield must be accurately controlled, for example, when staging multiple LWFA devices in series.

DOI: 10.1103/PhysRevSTAB.9.031303 PACS numbers: 41.75.Jv, 52.38.Kd, 42.55.Lt

I. INTRODUCTION

Laser-wakefield acceleration (LWFA) has demonstrated very high acceleration gradients in numerous experiments [1]. LWFA is typically initiated by sending a few tens of terawatt (TW) laser pulse into a plasma to create longitudinal plasma waves or wakefields [2]. These waves travel at near the speed of light and can accelerate electrons trapped within their potential well. When the laser pulse length τ_L is less than of order $\lambda_p/2c$, where λ_p is the plasma wavelength and c is the speed of light, this wakefield generation is referred to as resonant LWFA.

In a variation of the LWFA method, called self-modulated LWFA (SM-LWFA) [3], the laser pulse length is much longer than $\lambda_p/2c$, but the laser intensity is still very high. This permits the laser electric field to feed energy into the wakefield via forward Raman scattering and/or a self-modulation instability. This enhances the wakefield formation process allowing much higher gradients to be produced compared to resonant LWFA. However, for wakefield amplitudes of interest, SM-LWFA is a highly nonlinear process that typically starts from noise, so that the phase of the resulting wake is essentially uncontrolled.

Wakefield formation in a plasma is also possible by using an ultrashort electron beam (e-beam) bunch rather than a laser pulse. This is referred to as plasma wakefield acceleration (PWFA) [4]. The formation mechanism in PWFA is analogous to resonant LWFA; hence, the resultant wakefields can have similar characteristics.

This paper presents the modeling analysis for a new method of laser-wakefield generation, which we call seeded SM-LWFA. (This concept was first introduced as ''stimulated LWFA'' [5]). It is essentially a hybrid of PWFA and SM-LWFA where an ultrashort e-beam bunch generates a wakefield in a plasma via PWFA. A laser pulse immediately follows the e-beam bunch and amplifies the wakefield via the SM-LWFA process.

The motivations for the development of this novel method are twofold. First, LWFA experiments are being conducted at the Brookhaven National Laboratory Accelerator Test Facility (BNL-ATF) that will use a TW CO_2 laser to drive the acceleration process [6]. However, the CO_2 laser pulse length is too long for resonant LWFA. Furthermore, conventional SM-LWFA is not feasible because simulations indicate at the present laser power levels that transverse wakefields tend to be generated rather than longitudinal ones. Seeded SM-LWFA circumvents these limitations by using an e-beam to initiate a longitudinal wakefield with amplitude much larger than the noise level, which the laser pulse can then amplify.

Second, the ultimate aim of the LWFA experiments at the ATF is to demonstrate efficient trapping and acceleration of electron microbunches while maintaining a narrow energy spread (i.e., monoenergetic). This is an important requirement for any practical laser-driven linear accelerator. The strategy being followed is the same one proved successful during the staged electron laser acceleration (STELLA) experiments [7]. STELLA demonstrated efficient trapping and monoenergetic acceleration using a two-stage laser acceleration system based upon inverse free electron lasers (IFEL) [8]. The first IFEL stage modulated the e-beam energy thereby creating a train of micro-

*Electronic address: wkimura@stioptronics.com

bunches. The second IFEL trapped and accelerated these microbunches. Inherent in this basic approach is the need to rephase the microbunches with the accelerating field in the second acceleration stage. This implies the need to control the phase of the accelerating field.

During resonant LWFA or PWFA, the phase of the generated wakefield should be closely correlated to a feature of the laser or *e*-beam pulse shape, respectively. (The former assumes the laser power is below the threshold for self-focusing of the laser beam in the plasma [9]). Hence, seeded SM-LWFA may also provide a means for generating wakefields whose phase is more controllable than in conventional SM-LWFA where the wakefield arises from noise. The ATF LWFA experiment, which is referred to as STELLA-LW where LW stands for laser wakefield, would be one of the first to investigate control of the wakefield phase in this manner.

Note that there is another potential method for controlling the phase and character of SM-LWFA by using a second low-intensity frequency-shifted laser pulse, which provides a seed for the main laser pulse self-modulation and does not rely on noise to generate the wakefields [10,11].

The next section reviews changes made to an existing LWFA model to simulate the seeding process and the affects of the amplified wakefield on witness electrons that follow the seed *e*-beam bunch. Section III presents the model predictions assuming the ATF linac and CO_2 laser characteristics. Conclusions follow in Sec. IV.

II. MODIFICATIONS TO LWFA MODEL

As explained, seeded SM-LWFA requires a seed *e*-beam bunch and laser pulse. A second *e*-beam bunch (''witness'' bunch) follows the seed and laser pulses to provide electrons that interact with the amplified wakefield.

The ATF linac is capable of providing two *e*-beam bunches separated by a short time interval (e.g., 10–20 ps) [12]. The first bunch serves as the seed and the second as the witness. The ATF can also send these dual bunches through a magnetic chicane such that the first bunch is compressed to less than 200 fs while the duration of the second bunch remains largely unchanged. This compression of the first bunch is necessary for efficient seed wake generation. The length of the second witness bunch is less critical.

A model to simulate LWFA generation using a CO_2 laser pulse was developed earlier in conjunction with analysis of another scheme called pseudoresonant LWFA [13]. This model is well suited for also simulating seeded SM-LWFA; however, it required two modifications. The first is to introduce a seed *e*-beam bunch whose wakes interact with the laser pulse propagating through the plasma. The second is to add the witness bunch. Because the formation of the wakefields and their amplification does not occur immediately after entering the plasma, it is important to include the effects of the plasma on the witness electrons before they reach the high-amplitude wakefields.

Equations (1)–(4) below are reproductions of Eqs. (4)–(7) from [13] except for the addition of a new term $\mathbf{j}_b$ in Eq. (3) that represents the current density of the seed *e*-beam bunch.

$$\frac{\partial \mathbf{p}}{\partial t} = e\mathbf{E} - mc^2\nabla\gamma, \tag{1}$$

$$\frac{\partial n}{\partial t} + \nabla\cdot(n\mathbf{v}) = 0, \tag{2}$$

$$\frac{\partial \mathbf{E}}{\partial t} = -4\pi e n\mathbf{v} + c\nabla\times\mathbf{B} - 4\pi\mathbf{j}_b, \tag{3}$$

$$\nabla\times\mathbf{E} = -\frac{1}{c}\frac{\partial \mathbf{B}}{\partial t}, \tag{4}$$

where e is the electron charge; $\mathbf{E}$ and $\mathbf{B}$ are the electric field and magnetic flux in the plasma, respectively; m is the mass of the electron; $\gamma = [1 + (\mathbf{p}/mc)^2 + |a|^2/2]^{1/2}$; n is the plasma electron density; and $\mathbf{p}$ and $\mathbf{v}$ are the electron momentum and velocity, respectively. The dimensionless envelope amplitude a of the laser pulse is related to the electric field of the laser pulse $\mathbf{E}_0$ by the expression

$$e\mathbf{E}_0/(m\omega_0 c) = \mathrm{Re}\{\mathbf{e}_0 a\exp[-i\omega_0 t + ik_0 z]\}, \tag{5}$$

where ω_0 and $k_0 = \omega_0/c$ are the frequency and wave number of the laser radiation, respectively. Here $\mathbf{e}_0$ is the unit vector of the laser polarization, which is assumed to be linear. The quantity a is assumed to vary slowly on the time and spatial scales ω_0^{-1} and k_0^{-1}, respectively.

Equations (1)–(4) describe the slowly varying motions and fields in the plasma. The seed *e*-beam is assumed to be relativistic with a current that is some given function of time and space, e.g., Gaussian.

As done in [13], we make a quasistatic approximation [14] by defining dimensionless coordinates moving with the laser pulse variables

$$\xi = k_{p0}(z - ct), \qquad \zeta = k_{p0}z, \qquad \boldsymbol{\rho} = k_{p0}\mathbf{r}_\perp, \tag{6}$$

where $k_{p0} = \omega_{p0}/c = (4\pi e^2 N_0/m)^{1/2}/c$ is the normalizing inverse space scale; N_0 is the unperturbed electron plasma density on the *e*-beam axis, $N_0 = n_0(r = 0)$; and $\mathbf{r}_\perp = \{x, y\} = r\{\cos\varphi, \sin\varphi\}$ is the radius vector in the radial direction r.

With the addition of the seed bunch, the linearized Eq. (16) of [13] for the wakefield potential variation $\delta\Phi$ becomes

$$\left\{\left(\frac{\partial^2}{\partial\xi^2} + \nu_0\right)(\Delta_\perp - \nu_0) - \frac{\partial \ln[\nu_0(\rho)]}{\partial\rho}\frac{\partial^2}{\partial\xi^2}\frac{\partial}{\partial\rho}\right\}\delta\Phi = \nu_0\left[(\Delta_\perp - \nu_0)\frac{|a|^2}{4} - N_b\right], \tag{7}$$

where $\nu_0(\rho) = n_0(\rho)/N_0$ is the normalized electron back-

ground density in the plasma channel; N_b is the normalized seed electron bunch density, $N_b = n_b(\xi, \rho, \zeta)/N_0$, [$\mathbf{j}_b = \{0, 0, j_{bz}\}$, $j_{bz} = en_b(\xi, \rho, \zeta)c$]; and $\Delta_\perp$ is the transverse part of the Laplacian operator. All other equations in the model have the same form as in [13].

To investigate the acceleration of relativistic electrons of the witness e-beam bunch in the wakefield we use the equations of motion in the form of [15]

$$\frac{dP_z}{d\tau} = F_z(\xi, \rho, \zeta), \tag{8}$$

$$\frac{d\mathbf{P}_r}{d\tau} = \mathbf{F}_r(\xi, \rho, \zeta), \tag{9}$$

$$\frac{d\xi}{d\tau} = \frac{P_z}{\sqrt{1 + P_z^2 + P_r^2}} - 1, \tag{10}$$

$$\frac{d\boldsymbol{\rho}}{d\tau} = \frac{\mathbf{P}_r}{\sqrt{1 + P_z^2 + P_r^2}}, \tag{11}$$

where P_z, $\mathbf{P}_r = \{P_x, P_y\}$ are components of momentum, longitudinal and perpendicular to the axis OZ, of an accelerating electron normalized to mc; $\tau = \omega_{p0}t$; and $\zeta = \xi + \tau$. The axial and radial components of the normalized force acting on the accelerating electron moving with velocity c along the OZ axis is a reasonable approximation for the relativistic witness e-beam bunch. These components can be expressed in terms of the normalized (to mc^2/e) wakefield potential $\Phi = 1 + \delta\Phi$ as follows:

$$F_z \equiv \frac{eE_z}{mc\omega_{p0}} = \frac{\partial\Phi}{\partial\xi}, \tag{12}$$

$$F_r \equiv \frac{eE_r}{mc\omega_{p0}} - \frac{eB_\varphi}{mc\omega_{p0}} = \frac{\partial\Phi}{\partial\rho}, \tag{13}$$

where $\mathbf{F}_r = \{F_x, F_y\} = F_r\{\cos\varphi, \sin\varphi\}$.

In the simulations that follow we make the simplifying assumption of an infinite uniform plasma density in all directions. As a result the laser beam will exhibit modest diffractive spreading over the short plasma lengths modeled since the propagation distance is less than the laser beam Rayleigh range. In actual experiments [6], a capillary discharge could be used to guide the laser beam over longer distances.

III. MODEL PREDICTIONS FOR SEEDED SM-LWFA

The conventions for describing the e-beam and laser beam are as follows. The laser beam amplitude a is given by

$$a(r, z = 0, t) = a_0 \exp\left[-\frac{r^2}{w_0^2} - \frac{(t - t_a)^2}{\tau_L^2} \right], \tag{14}$$

and the e-beam density distribution is described as

$$n_b(r, z = 0, t) = n_{b0} \exp\left[-\frac{r^2}{2\sigma_e^2} - \frac{(t - t_b)^2}{2\tau_e^2} \right], \tag{15}$$

where t_a and t_b represent the delay times between the various pulses; $\sigma_e \equiv \sigma_{e\text{-seed}}$, $t_b \equiv t_{b\text{-seed}}$, and $\tau_e \equiv \tau_{e\text{-seed}}$ for the seed e-beam bunch; and $\sigma_e \equiv \sigma_{e\text{-witness}}$, $t_b \equiv t_{b\text{-witness}}$, and $\tau_e \equiv \tau_{e\text{-witness}}$ for the witness e-beam bunch. These seemingly mixed conventions were adopted because of their prevalent usage within the laser (for a) and accelerator (for n_b) communities. For example, w_0 is the usual waist of the laser beam focus, whereas σ_e is the rms size of the e-beam.

Table I lists the parameter values used in the model, which were chosen to simulate the approximate anticipated conditions at the ATF when utilizing the magnetic chicane to compress the seed e-beam bunch. As mentioned, the assumption is made that the plasma density is uniform over the entire plasma length; in reality, it may vary longitudinally when the capillary is short, e.g., 3–4 mm.

One important parameter to note is the plasma density, which is approaching 10^{17} cm^{-3}. This is nearly $10\times$ higher than the density required for pseudoresonant LWFA [13]. It can be higher because the compressed seed e-beam bunch length, of order ~100–200 fs, is short enough for efficient seed wake generation at this higher density.

In the model predictions that follow, two cases are examined where the parameters are essentially the same except for differences in the temporal position of the seed bunch $t_d = t_{b\text{-seed}} - t_a$ within the laser pulse envelope. The delay time t_d is measured between the peaks of the laser pulse and the seed e-beam bunch at the capillary entrance. This shows the sensitivity of the seeding process to this time delay.

A. Time delay between laser and seed pulses t_d = 2.97 ps

Figures 1–5 show the results for the case when t_d = 2.97 ps. In Fig. 1, the peak of the wakefield potential and the laser field maximum on axis are shown. The maximum of the laser field at the plasma boundary is chosen to be at $\xi = \xi_a = 200$. The seed e-beam bunch propagates ahead of the laser pulse at $\xi_b = 250$, which corresponds to a time delay between the laser pulse and seed e-beam bunch of t_d = 2.97 ps. This can be seen more clearly in Fig. 2, where the dashed line represents the laser pulse envelope at the plasma entrance ($z = 0$). The oscillating (red) line just below is the envelope after the pulse propagates in the plasma a distance z = 2.62 mm. It is slightly lower because of some defocusing of the laser beam caused by diffraction. (For the conditions simulated, depletion of laser pulse energy is negligible.) More importantly, it shows the modulation characteristics of a strong interaction with the seed wake. This results in a growth of the

TABLE I. Laser and plasma parameters used in seeded SM-LWFA simulations.

Parameter	Value
Laser wavelength, λ_L	10.6 μm
Laser pulse duration, τ_L[a]	8.44 ps
Laser peak power, P_L	0.5 TW
Laser pulse energy, E_L	5.3 J
Laser beam focus radius, w_0	111 μm
Laser beam Rayleigh range, z_R	3.64 mm
Normalized laser field strength, a_0	0.462
Plasma length[b]	2–3 mm
Plasma density on axis, n_0[c]	0.89×10^{17} cm^{-3}
P_L/P_{crit} (for self-focusing)	0.265
Time delay between peak of laser pulse and peak of seed e-beam bunch, t_d	2.97 or 8.91 ps
E-beam energy (seed and witness), E_{inj}	64 MeV
Seed e-beam intrinsic energy spread [%]	$\ll 1\%$[d]
Seed e-beam bunch charge	199 pC
Seed e-beam bunch length, $\tau_{e\text{-seed}}$	118 fs
Seed e-beam focus size at capillary, $\sigma_{e\text{-seed}}$	50 μm
Witness e-beam intrinsic energy spread [%]	0.05
Witness e-beam bunch charge	$\ll$ 500 pC[e]
Witness e-beam bunch length, $\tau_{e\text{-witness}}$	1.23 ps
Witness e-beam focus size at capillary, $\sigma_{e\text{-witness}}$	20 μm
Time delay between seed and witness e-beam bunches, τ_d	6–21 ps

[a]The full-width-at-half-maximum pulse duration of the laser intensity is equal to $\tau_{\text{FWHM}} = 2\sqrt{\ln 2}\ \tau_{\text{L}} = 9.93$ ps.
[b]The plasma length is assumed to be the same as the capillary length.
[c]The plasma density is assumed uniform over the entire plasma length.
[d]The seed e-beam propagates with constant velocity determined by its energy without changing its shape, so the results do not depend on the initial energy spread.
[e]Not critical assuming loading effects can be ignored.

wakefield potential as shown plotted to the right of the seed bunch in Fig. 2.

Note that the wakefield potential over the first 1.5 mm propagation distance (see Fig. 1) is not the pure amplitude of the plasma wave (which is responsible for accelerating the electrons), but also reflects the ponderomotive potential of the laser pulse.

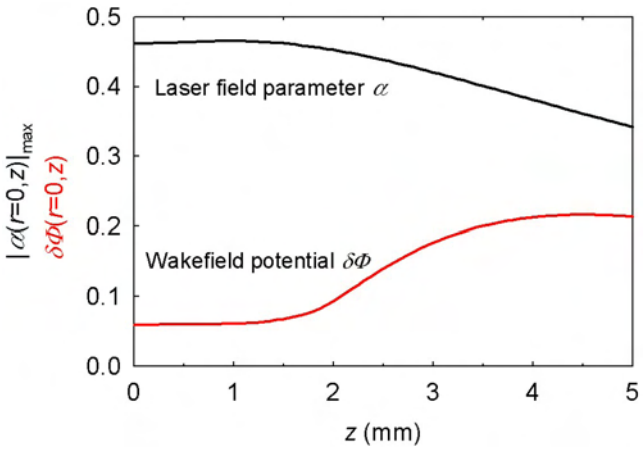

FIG. 1. (Color) Model prediction for the maximum of laser field parameter $|a(r = 0, z)|_{\max}$ and wakefield potential $\delta\Phi_{\max}$ ($r = 0, z$) as a function of distance along the plasma for $t_d = 2.97$ ps.

In Fig. 3, we see that the wakefields are predominately longitudinal after a propagation distance of 2.62 mm. They remain longitudinal even for distances over 5 mm (not shown). The radial extent of the strongest wakefields ex-

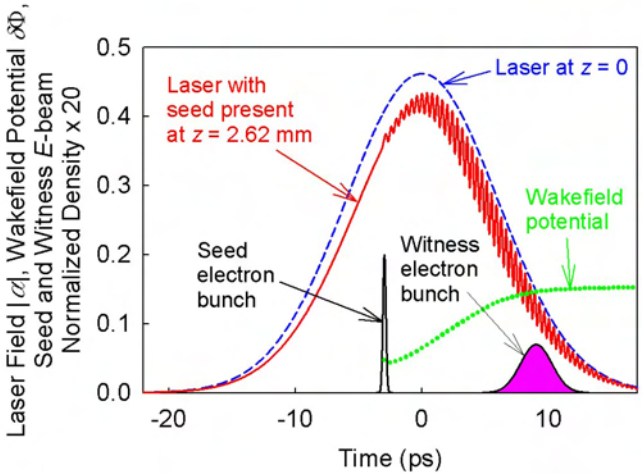

FIG. 2. (Color) Model prediction for laser field parameter $|a(r = 0)|$ and wakefield potential $\delta\Phi$ ($r = 0$) as a function of time for $z = 2.62$ mm and $t_d = 2.97$ ps. Also plotted are the seed and witness e-beam bunch positions for $\tau_d = 12$ ps and $|a(r = 0, z = 0)|$.

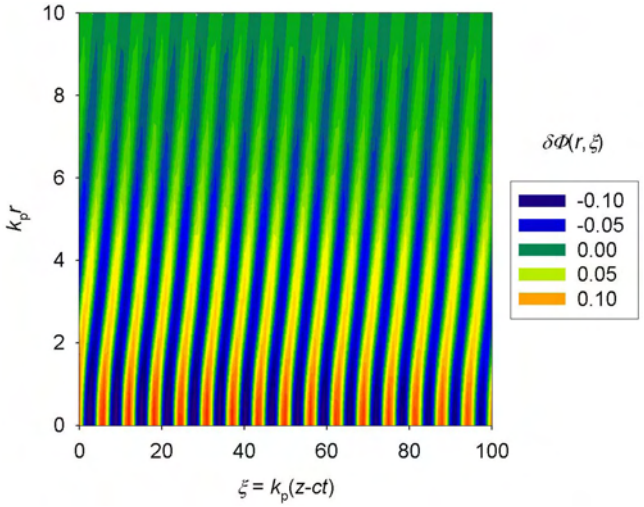

FIG. 3. (Color) Model prediction for wakefield potential distribution $\delta\Phi(r, \xi)$ plotted after a propagation distance of 2.62 mm for $t_d = 2.97$ ps.

tends to approximately $k_p r = 3$. For a plasma density of 8.9×10^{16} cm^{-3}, the plasma wavelength $\lambda_p = 112$ μm and $k_p = 2\pi/\lambda_p = 561$ cm^{-1}. Hence, $k_p r = 3$ corresponds to a radial distance of 53 μm. Thus, the witness e-beam bunch rms radius should be less than this distance.

These figures demonstrate effective wakefield generation after propagation over the first 2 mm (representing the initial stage of self-modulation development). Moreover, the wakefields generated are primarily longitudinal rather than transverse. This overcomes the problem that is predicted to appear if the ATF CO_2 laser pulse alone is used to generate wakefields via SM-LWFA.

Figure 2 also illustrates a typical time separation τ_d between the seed and witness e-beam bunches, and their temporal positions relative to the laser pulse. In this particular case, $\tau_d = 12$ ps.

Figure 4 presents the predicted energy spectrum of the witness bunch for $\sigma_{e\text{-witness}} = 20$ μm, $\tau_{e\text{-witness}} = 1.23$ ps, and an acceleration length $L_{\text{acc}} = 2$ mm. Plotted are the spectrums for different τ_d between the seed and witness e-beam bunches. The intrinsic energy spread of the injected witness e-beam bunch is neglected in this figure. (Other model runs show that a small intrinsic energy spread of the witness e-beam, which is much smaller than the final energy spectrum, does not change the energy modulation characteristics of the witness bunch.) A double-peak energy spectrum is observed, which is evidence of sinusoidal energy modulation [16]. This peak modulation appears to reach a steady-state maximum value of $\approx \pm 1$ MeV for time separations greater than $\tau_d \sim 10$ ps. This implies the time delay between the seed and witness e-beam bunches is not critical and delays of $\tau_d \approx 10$–20 ps are acceptable.

An acceleration distance of 2 mm is comparable to the dephasing length calculated by using the average phase velocity of the wakefield at $z \approx 2$ mm, i.e., $L_{dph} = \lambda_p \bar{\gamma}_{ph}^2 \cong 1.8$ mm with $\bar{\gamma}_{ph} \cong 4$, which is derived from analysis of the wakefield phase obtained in separate calculations. (Note the relativistic parameter associated with the group velocity of the laser pulse is $\gamma_g = \omega_0/\omega_p \cong 10.6$.) This explains why the spectra in Fig. 4 are more symmetrical than those that will be shown later for $L_{\text{acc}} = 3$ mm.

The spectrum for the shortest time separation ($\tau_d = 6$ ps) displays a small peak at the mean e-beam energy (i.e., 64 MeV). This is caused by a small number of witness electrons that are located on the low amplitude wakefield near the seed e-beam bunch position. This peak will also be clearly seen later in Fig. 5.

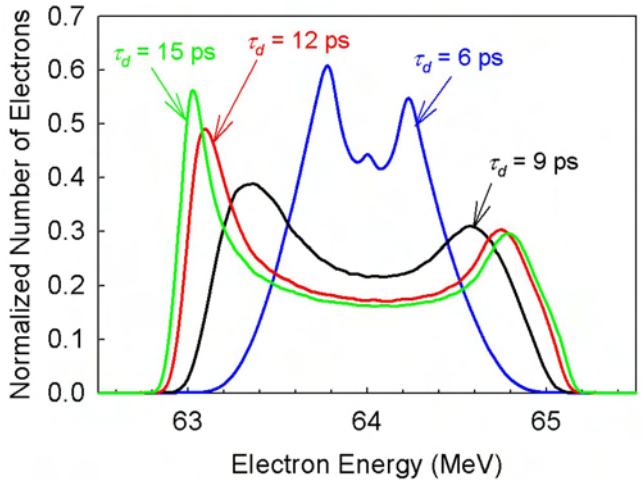

FIG. 4. (Color) Model prediction for energy spectrum of witness bunch for $t_d = 2.97$ ps and different time delays between the seed and witness e-beam bunches for an acceleration length $L_{\text{acc}} = 2$ mm.

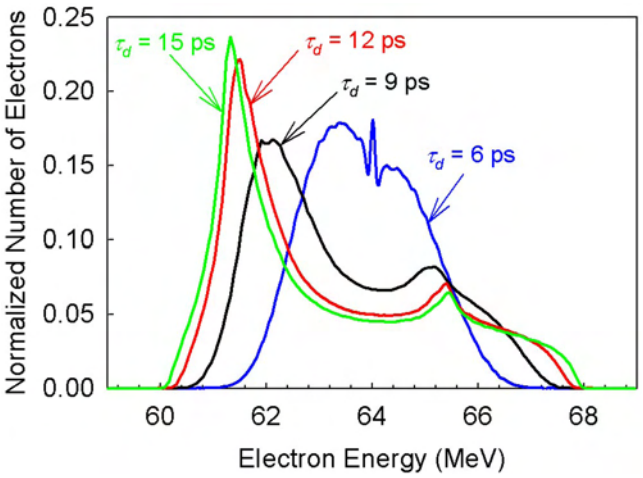

FIG. 5. (Color) Model prediction for energy spectrum of witness bunch for $t_d = 2.97$ ps and different time delays between the seed and witness e-beam bunches for an acceleration length $L_{\text{acc}} = 3$ mm.

Increasing the acceleration length by 50% to $L_{\rm acc} = 3$ mm, the predicted energy spectra are shown in Fig. 5. The maximum amount of modulation has increased by ~400% to nearly ±4 MeV and the spectra have become considerably asymmetric in shape. The more pronounced asymmetry of the spectrum (in comparison with Fig. 4) is a consequence of the acceleration distance, $L_{\rm acc} = 3$ mm, exceeding the dephasing length, $L_{\rm dph} \cong 1.8$ mm, which leads to deceleration of a substantial part of the electrons in the witness bunch.

B. Time delay between laser and seed pulses $t_d = 8.91$ ps

Figure 6 shows the relationship between the various pulses and fields when the time delay between the laser and seed pulse is increased to $t_d = 8.91$ ps. Comparing Fig. 6 with Fig. 2, this is achieved by having the seed *e*-beam bunch arrive earlier with respect to the laser pulse. The witness *e*-beam bunch is essentially in the same time location with respect to the laser pulse. Moving the seed bunch earlier allows the wakefields to begin growing earlier within the laser pulse thereby resulting in higher amplitude of the wakefield potential, cf. wakefield potential plots in Figs. 2 and 6.

Figure 7 shows the energy spectrum for different time separations between the seed and witness *e*-beam bunches for a witness *e*-beam bunch with an intrinsic energy spread of $\sigma_{\mathbf{E}} = 0.05\% E_{\rm inj}$ and an acceleration length $L_{\rm acc} = 3$ mm. The maximum energy modulation has now increased to over ±6 MeV. This corresponds to an acceleration gradient of 2 GeV/m.

There is also a larger concentration of decelerated electrons at approximately 60.5 MeV due to increased decelerating forces (as compared with Figs. 4 and 5) for the main portion of electrons in the witness *e*-beam bunch because the acceleration length exceeds the dephasing length.

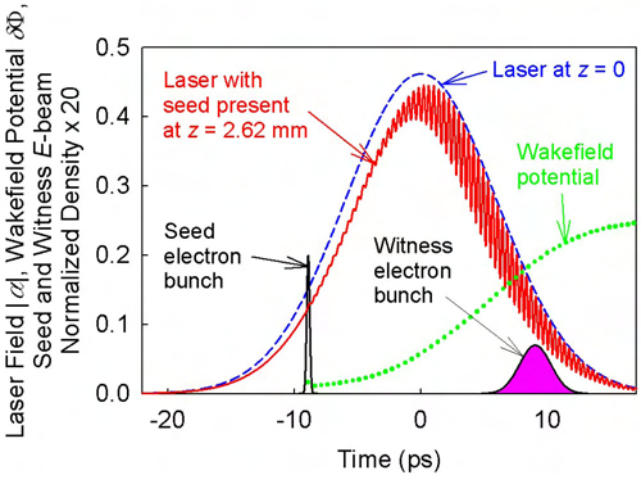

FIG. 6. (Color) Model prediction for laser field parameter $|a(r=0)|$ and wakefield potential $\delta\Phi(r=0)$ as a function of time for $t_d = 8.91$ ps. Also plotted are the seed and witness *e*-beam bunch positions for $\tau_d = 17$ ps and $|a(r=0, z=0)|$.

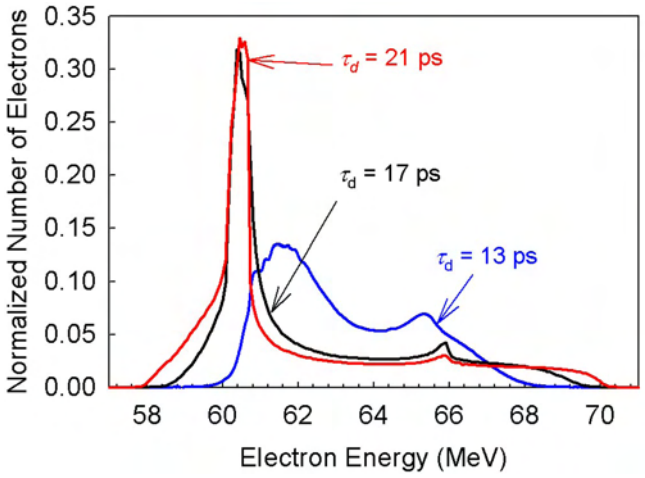

FIG. 7. (Color) Model prediction for energy spectrum of witness bunch for $t_d = 8.91$ ps and different time delays between the seed and witness *e*-beam bunches for an acceleration length $L_{\rm acc} = 3$ mm.

Moreover, in our simulations the witness bunch length (~ 1000 μm) is much longer than the plasma wavelength (~ 100 μm), which results in the energy modulation seen in the figures. Efficient, monoenergetic acceleration is possible if the witness bunch length can made of order 1/10 the plasma wavelength. This should be achievable using a technique similar to the STELLA experiment [16], where the witness electrons are energy modulated in a short-length, seeded SM-LWFA device and allowed to form a train of microbunches. These microbunches can be subsequently sent into a second LWFA device and rephrased with the plasma wave for maximum acceleration.

IV. CONCLUSION

A novel method for generating wakefields has been analyzed, which combines PWFA and SM-LWFA. It provides several potential benefits: (1) It enables strong wakefield generation that is comparable to conventional SM-LWFA, but where the laser pulse characteristics are insufficient to initiate the SM-LWFA process by using the laser pulse only. (2) The longitudinal structure of the wakefield is tied closely to the seed *e*-beam bunch, which may enable more precise control of the wakefield phase, thereby facilitating staging of LWFA devices. (3) For the conditions at the ATF, seeded SM-LWFA permits operation at considerably higher plasma densities than pseudoresonant LWFA, thereby easing the operational requirements of a capillary discharge.

The STELLA-LW experiment plans a proof-of-principle demonstration of seeded SM-LWFA in the near future [17] with the goal of observing the type of energy modulation

predicted in this paper. Future experiments would build upon this proof-of-principle experiment to demonstrate microbunch formation, staging, and monoenergetic acceleration.

ACKNOWLEDGMENTS

This work was supported by the U.S. Department of Energy, Grant No. DE-FG02-04ER41294.

[1] See, for example, W. P. Leemans and E. Esarey, in *Advanced Accelerator Concepts: Eighth Workshop*, edited by W. Lawson, C. Bellamy, and D. Brosius, AIP Conf. Proc. No. 472 (American Institute of Physics, New York, 1999), p. 174.

[2] T. Tajima and J. M. Dawson, Phys. Rev. Lett. **43**, 267 (1979); L. M. Gorbunov and V. I. Kirsanov, Sov. Phys. JETP **66**, 290 (1987).

[3] N. E. Andreev, L. M. Gorbunov, V. I. Kirsanov, A. A. Pogosova, and R. R. Ramazashvili, Pis'ma Zh. Eksp. Teor. Fiz. **55**, 551 (1992) [JETP Lett. **55**, 571 (1992)].

[4] P. Chen, J. M. Dawson, R. W. Huff, and T. Katsouleas, Phys. Rev. Lett. **54**, 693 (1985).

[5] L. C. Steinhauer, W. D. Kimura, and R. N. Agarwal, in *Proceedings of International Conference on Lasers 2001*, edited by V. J. Corcoran and T. A. Corcoran (STS Press, McLean, 2002), pp. 159–163.

[6] W. D. Kimura, N. E. Andreev, M. Babzien, I. Ben-Zvi, D. B. Cline, C. E. Dilley, S. C. Gottschalk, S. M. Hooker, K. P. Kusche, S. V. Kuznetsov, R. H. Pantell, I. V. Pavlishin, I. V. Pogorelsky, A. A. Pogosova, L. C. Steinhauer, A. Ting, V. Yakimenko, A. Zigler, and F. Zhou, IEEE Trans. Plasma Sci. **33**, 3 (2005).

[7] W. D. Kimura, M. Babzien, I. Ben-Zvi, L. P. Campbell, D. B. Cline, C. E. Dilley, J. C. Gallardo, S. C. Gottschalk, K. P. Kusche, R. H. Pantell, I. V. Pogorelsky, D. C. Quimby, J. Skaritka, L. C. Steinhauer, V. Yakimenko, and F. Zhou, Phys. Rev. Lett. **92**, 054801 (2004).

[8] R. B. Palmer, J. Appl. Phys. **43**, 3014 (1972).

[9] P. Sprangle, E. Esarey, A. Ting, and G. Joyce, Appl. Phys. Lett. **53**, 2146 (1988).

[10] N. E. Andreev, L. M. Gorbunov, and V. I. Kirsanov, Fiz. Plazmy **21**, 872 (1995) [Plasma Phys. Rep. **21**, 824 (1995)]; Phys. Plasmas **2**, 2573 (1995).

[11] M. Fomyts'kyi, C. Chiu, M. Downer, and F. Grigsby, Phys. Plasmas **12**, 023103 (2005).

[12] F. Zhou, D. Cline, M. Babzien, V. Yakimenko, and W. D. Kimura, in *Proceedings of the Particle Accelerator Conference, Knoxville, TN, 2005* (IEEE, Piscataway, NJ, 2005), pp. 2312–2314 [IEEE Cat. No. 05CH37623C].

[13] N. E. Andreev, S. V. Kuznetsov, A. A. Pogosova, L. C. Steinhauer, and W. D. Kimura, Phys. Rev. ST Accel. Beams **6**, 041301 (2003).

[14] P. Sprangle, E. Esarey, and A. Ting, Phys. Rev. Lett. **64**, 2011 (1990).

[15] N. E. Andreev, S. V. Kuznetsov, I. V. Pogorelsky, Phys. Rev. ST Accel. Beams **3**, 021301 (2000).

[16] W. D. Kimura, L. P. Campbell, C. E. Dilley, S. C. Gottschalk, D. C. Quimby, M. Babzien, I. Ben-Zvi, J. C. Gallardo, K. P. Kusche, I. V. Pogorelsky, J. Skaritka, V. Yakimenko, D. B. Cline, F. Zhou, L. C. Steinhauer, and R. H. Pantell, Phys. Rev. ST Accel. Beams **7**, 091301 (2004).

[17] W. D. Kimura, N. E. Andreev, M. Babzien, I. Ben-Zvi, D. B. Cline, C. E. Dilley, S. C. Gottschalk, S. M. Hooker, K. P. Kusche, S. V. Kuznetsov, I. V. Pavlishin, I. V. Pogorelsky, A. A. Pogosova, L. C. Steinhauer, A. Ting, V. Yakimenko, A. Zigler, and F. Zhou, Phil. Trans. R. Soc. A **364**, 611 (2006).